Forensic Science International: Synergy 6 (2023) 100306

Contents lists available at ScienceDirect

Forensic Science International: Synergy

journal homepage: www.sciencedirect.com/journal/forensic-science-international-synergy

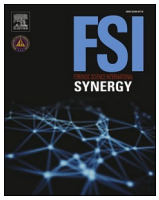

Interpol review of paint, tape, and glass evidence 2019–2022

Jose Almirall [a,*], Tatiana Trejos [b]

[a] Florida International University, Department of Chemistry and Biochemistry, Center for Advanced Research in Forensic Science, Miami, FL, USA
[b] West Virginia University, Department of Forensic and Investigative Science, USA

1. Introduction

This review paper covers advances in scientific methods applied to Glass, Paint, and Tape reported since the 19th Interpol Forensic Science Symposium in October 2019. The review includes peer-reviewed literature, published reports, books, and book chapters on the subjects. Forensic examiners should also be aware of the publication of standard practices, guides, and test methods (e.g., ASTM) and the developments within the manufacturing industries, including production volumes, production locations, and the current trends in the manufacture of these widely used materials.

The leading peer reviewed journals reviewed for this paper were Forensic Chemistry, the Journal of Forensic Sciences, and Forensic Science International. In addition, more than seventy (70) different analytical chemistry or other science journals have published peer-reviewed communications on the advances in forensic paint, tape, and glass examinations in the past 3 years.

Jeff Teitelbaum, Forensic Research Librarian at the Florida International University's Global Forensic and Justice Center, contributed with the primary literature search using keywords for forensic paint, glass, and tape. In addition, literature from several search engines such as Science Direct, SciFinder, Web of Science, and Google Scholar from the last three years were also considered. The literature review is primarily focused on peer-reviewed articles and books published since the summer of 2019 to the summer of 2022.

This review made evident a growing interest in the trace evidence community on chemometrics and statistical interpretation of the data. The increasing literature in this field can facilitate wider adoption in operational forensic laboratories. Several studies have emphasized using statistics for pattern recognition, data reduction and classifications, optimization and validation of analytical procedures, and assessing the evidential value of the traces. An array of methods was reported, including principal component analysis, discriminant analysis, neural networks, and likelihood ratios, to mention some.

1.1. Books, review articles, and consensus-based standards

Various books and book chapters on glass, paint, tape, and, more generally, trace materials evidence were published in the review period:

1) The first edition of the Handbook of Trace Evidence Analysis contains seven chapters on trace evidence, including five pertinent to this review [1]. Chapter 1 focuses on trace evidence recognition, collection, and preservation. Chapter 2 thoroughly reviews polarized light microscopy for trace evidence, while Chapters 3 and 6 focus on paint, polymers, and glass evidence, respectively. Finally, Chapter 7 provides a discussion of interpretation approaches in trace evidence.
2) The second edition of Paint Analysis: The Handbook for Study and Practice discusses in detail the analysis of paints and coatings, emphasizing analytical testing, sampling, failure analysis, and quality control in the coating industry [2]. Part IV of the book covers 12 chapters dedicated to analytical methods, including optical light microscopy, fluorescence microscopy, infrared spectroscopy, surface infrared spectroscopy, infrared microscopy, Raman spectroscopy, time-of-flight secondary ion mass spectrometry, scanning electron microscopy, electron microanalysis, X-ray photoelectron spectroscopy, thin-layer chromatography, and gas chromatography-mass spectrometry.
3) The book Resins for Waterborne Coatings presents a comprehensive discussion of market trends, regulations, industry terminology, and the chemistry and formulations of various resins such as alkyds, epoxy, silicone, alkali silicates, amino resins, and hardeners [3].
4) Chapter 21 of the third edition of Forensic Science: The Basics by Siegel and Mirakovits discusses paint and fiber analysis fundamentals, including some case studies [4].
5) Chapter 14 of the 13th edition of Criminalistics: An Introduction to Forensic Science, by Saferstein and Roy, provides an overview of paint, soil, and metal evidence [5].
6) In Chapter 8 of the Analytical Pyrolysis Handbook: Examination of Forensic Evidence, the authors describe the application and interpretation of Py-GC-MS data for the forensic examination of various trace materials, including architectural, industrial, and automotive paint, adhesives, rubbers, and plastics, to mention some [6].

* Corresponding author.
E-mail addresses: jalmiral@nsf.gov (J. Almirall), tatiana.trejos@mail.wvu.edu (T. Trejos).

https://doi.org/10.1016/j.fsisyn.2022.100306

7) Chapter 14 of the Practical Forensic Microscopy: A Laboratory Manual outlines a laboratory exercise to develop basic skills on general characteristics of paint by cross-sectioning, solubility testing, and microscopic examination [7].
8) Chapter 5 of Crime Scene Management within Forensic Science discusses the fundamentals of composition and analysis of paint, soil, and glass evidence [8].
9) In Chapter 6 of the Forensic Science Handbook, Suzuki provides a comprehensive discussion of the theory, instrumentation, and interpretation of FTIR spectra, with two sections dedicated to paints, polymers, and adhesives [9].
10) In Chapter 2 of the Forensic Science Handbook, Wright and Thornton describes the forensic examination of pains [10].

Also, various review articles were published in the past three years. In 2020, Trejos et al. wrote an overarching review on five trace subdisciplines: hair, fiber, tape, paint, and glass [11]. This review discusses the current state of trace evidence, along with a historical evaluation of the scientific foundations and advancements in the field.

In the same year, Lavine et al. presented a literature review of the criteria used in forensic science to compare IR spectra [12]. The article focuses on library searching (spectra comparison to a database), pattern recognition for discrimination purposes, and the use of likelihood ratio to assess the strength of spectral similarity in comparative analysis. Various similarity metrics algorithms for library searching were discussed, including the correlation coefficients calculated from the mean-centered absorbances or the absorbance values, the Manhattan city block distance (absolute absorbance differences), and the Euclidean distance. The authors recommended caution when using the hit quality index to account for sample contamination, signal to noise, instrument type, and measurement geometry. Linear and quadratic discriminant analysis, support vector machines, SIMCA, and principal component analysis are among the pattern recognition algorithms discussed in this manuscript.

Duarte et al. published a comprehensive review of the automotive paint analysis literature from 2010 to 2019, focusing on analytical instrumentation and chemical analysis [13]. Among the methodologies listed were the most utilized PLM, FTIR, Py-GC/MS, SEM-EDS, UV–Vis, and XRF, and other newer methodologies in paint examinations using Near Infrared, ICP-OES, ICP-MS, DART-MS, Fluorescence Microscopy, Optical Coherence Tomography, SERS, and LIBS. Kaur et al. also published a literature review on automotive paint focusing on instrumental analysis from 2015 to 2020 [14]. Like the Duarte et al. review, the authors agree on the techniques and relative frequency of publications per methodology, with a large overlap in the citations provided.

Finally, in 2022, Bailey et al. published a review of analytical chemistry focused on surface analysis in forensic science, including a section on paint and glass literature in the past decade [15].

Among some of the consensus-based standard guidelines and practices that were recently published or updated during this review period are:

1) ASTM E2808-21a Standard Guide for Microspectrophotometry in Forensic Paint Analysis [16].
2) ASTM E1610-18 Standard Guide for Forensic Paint Analysis and Comparison [17].
3) ASTM E2937-18 Standard Guide for Using Infrared Spectroscopy in Forensic Paint Examinations [18].
4) ASTM E3234-20 Standard Practice for Forensic Paint Analysis Training Program [19].
5) ASTM E3296-22 Standard Guide for Using Pyrolysis Gas Chromatography and Pyrolysis Gas Chromatography-Mass Spectrometry in Forensic Polymer Examinations [20].
6) ASTM D5380-21 Standard test method for identification of crystalline pigments and extenders in paint by X-ray diffraction analysis [21].
7) ASTM E3296-22 Standard Guide for Using Pyrolysis Gas Chromatography and Pyrolysis Gas Chromatography-Mass Spectrometry in Forensic Polymer Examinations [22].
8) ASTM E3260-21 Standard Guide for Forensic Examination and Comparison of Pressure Sensitive Tapes [23].
9) ASTM E3233-20 Standard Practice for Forensic Tape Analysis Training Program [24].
10) ASTM E1967-19 Standard Test Method for the Automated Determination of Refractive Index of Glass Samples Using the Oil Immersion Method and a Phase Contrast Microscope [25].
11) ASTM E2330-19 Standard Test Method for Determination of Concentrations of Elements in Glass Samples Using Inductively Coupled Plasma Mass Spectrometry (ICP-MS) for Forensic Comparisons [26].

A list of the ASTM standards that have been approved by the Organization of Scientific Area Committees (OSAC) can be found on the Trace Materials Subcommittee of the OSAC: https://www.nist.gov/organization-scientific-area-committees-forensic-science/trace-materials-subcommittee.

Moreover, the ENSI Paint and Glass Working Group has developed the following best practice manual and guidelines:

12) EPG-BPM-001 Best Practice Manual for the forensic examination of paint [27].
13) EPG Guideline-001 Guideline for the initial inspection search and recovery of forensic paint samples [28].
14) EPG Guideline-002 Guideline for the forensic examination of paint by FT infrared spectroscopy [29].
15) EPG Guideline-003 Guideline for the forensic examination of paint by Raman spectroscopy [30].
16) EPG Guideline-004 Guideline for the forensic examination of paint by SEM-EDS [31].
17) EPG Guideline-005 Guideline for the forensic examination of paint by Pyrolysis GC-MS [32].

1.2. Paint evidence

1.2.1. Analytical methods and spectral comparisons

FTIR spectroscopy is an informative and rapid technique that enables the non-destructive analysis of small samples. Thus, it is not surprising that IR spectroscopy continues as one of the techniques more widely reported in the literature for paint examinations, although many other techniques are being investigated. Raman spectroscopy is the second most used technique described in the paint literature.

In 2021, Kwofie et al. demonstrated the advantages of a sample preparation approach that avoids embedding media and therefore prevents spectral interference from the epoxy casting material [33]. In this study, they perform the paint cross-section by securing the paint chip between two rigid pieces of polyethylene before cutting in the microtome. Then, the authors performed IR image maps of the automotive paint fragments. The spectra of the individual paint layers were reconstructed by alternating least squares (ALS) and compared against a library. Superior library matches were feasible with the proposed method compared to embedding the paint in epoxy for microtome cross-sectioning. In a follow-up study, the same group evaluated the FTIR and machine learning algorithms for the make/model classification of OEM automotive paints [34]. The validation dataset consisted of 4-layer paints from the RCMP collection from 26 OEM vehicles (2000–2006). The results showed that the machine learning approach using search prefilters to focus on binder signatures could be applied to the ALS reconstructed IR spectra of each layer to identify OEM paint manufacture information.

In 2021, Suzuki published a series of papers describing his work on the characterization of perylenes organic pigments by FTIR [35–38]. The survey included OEM automotive paints from 1974 to 2019,

obtained from the CTS Reference Collection of Automotive Paints, paint manufacturers, the FBI Laboratory National Automotive Paint File, local automobile rebuild shops, and vehicles in salvage yards. In the first manuscript, the author thoroughly discusses the FTIR spectra and main functional groups of five perylenes, information about finishes containing these pigments, and strategies to identify the perylenes when present with other components, including red mica. This study was focused on Perylene Red Y (C.I. Pigment Red 224), which was found mainly in vehicles manufactured before 1989 [35].

A second manuscript describes the characterization of Perylene Maroon (C.I. Pigment Red 179), a pigment commonly found in red o maroon metallic basecoats [36]. The study also describes the IR identification of red alumina pearlescent pigment found in finishes manufactured after 2000. The IR spectra of 143 red or maroon metallic OEM basecoats were examined, and the Perylene Maroon was found to be prevalent in these finishes. A third publication reports the identification of Perylene Bordeaux (C.I. Pigment Violet 29) [37]. This pigment was found in both metallic and nonmetallic automotive finishes with maroon hues. Unlike the other two perylenes previously discussed, perylene Burdeaux is used in light to medium amounts and combined with other pigments, making the IR identification less straightforward. A variety of examples of IR spectra with pigment combinations are illustrated and discussed. The fourth perylene, Perylene Red (C.I. Pigment Red 178), was found exclusively in nonmetallic finishes with red hues [38]. This pigment was used in OEM finishes from 1984 until the early 1990s. Overall, this series of publications provide information about the use of IR spectra to identify these commonly used pigments, along with strategies that can be used in casework for comparative analyses and vehicle identifications.

Various paint discrimination studies have been reported in this period. In 2020, the Forensic Chemistry and Physics Laboratory in Singapore conducted an in-house population study of 256 vehicle paints of six major colors [39]. After examination and comparison by microscopy, SEM-EDS, and FTIR, 99.98% of the paints were differentiated. In addition, a population study of the automotive distribution in Singapore was obtained from data from the local transport authority, surveys conducted on random vehicles, and the laboratory collection of automotive paint samples. Distributions of makes were compared to those reported in the literature for Australia, US, and Canada, with notable differences observed. Higher relative percent of Toyota and Honda makes were documented in the Singapore survey, while no General Motors were observed, which was predominant in the other compared regions. Substantial differences were also observed in the frequency of decorative flakes on black topcoats compared to other published studies, indicating the importance of using region-relevant information to interpret paint evidence.

Sharma et al. [40] studied the discrimination of sixty red spray paints from 20 manufacturers by ATR-FTIR and principal component analysis (PCA). Data pre-processing for PCA included baseline offset and linear baseline correction, smoothing with Savitzky–Golay and second polynomial order, normalization by range, and multiplicative scatter correction (MSC). PCA achieved correct discrimination of all samples and correct classification of eight blind paints. Among the substrates examined, cement, fabrics, and paper produced poor spectra due to the matrix interferences, while gloves, metal, plastic, leather shoes, tile, wood, and hair substrates all rendered good results and similar spectra to the neat spray paints. Good reproducibility was reported for the intra-brands samples (three per brand).

He et al. reported using Microscopic Laser Raman spectroscopy (MLRM) to compare white architectural paints [41]. Analyzing 252 architectural paints from seven manufacturers using Bayes discriminant analysis yielded 100% discrimination of the samples. The data preprocessing that provided the best results included Newton interpolation polynomial correction combined with Savitzky-Golay and polynomial smoothing. Principal component analysis was used to reduce data dimensionality, and Bayes discriminant analysis (BDA) and multilayer perceptron neural network (MLP) were evaluated for sample classification. The study demonstrated the utility of MLRM for rapid screening of architectural paints and the use of statistical models for classification purposes.

Duarte et al. analyzed a collection of 143 white automotive paints by ATR-FTIR and coupled microscopy [42]. Spectra were collected from vehicles involved in car accidents and analyzed in five locations. Principal component analysis (PCA) and partial least squares discriminant analysis (PLS-DA) was used for sample classification. The model classification accuracy range from 79% to 100%, depending on the set used for calibration, testing, or validation.

In a study by Verma et al., a set of 40 automotive samples from two Indian manufacturers were evaluated by solubility tests. A subset of 10 samples was further examined by ATR-FTIR [43]. Samples from the two manufacturers were differentiated based on solubility and chemical composition. In another study by the same group, a small set of nine paint samples collected from Indian vehicles manufactured by Maruti Suzuki was analyzed by SEM-EDS. All paints were cross-sectioned, embedded in epoxy, and reported to contain two layers. The authors say the presence of thulium, which they hypothesized may be linked to this manufacturer [44].

In a research study by Sabaradin et al., 80 simulated automotive paint samples were analyzed using Py-GC-MS, with an emphasis on evaluating the discrimination of paint transfers of two layers: base coat and primer [45]. The simulated samples were prepared on aluminum sheets, where ten different primers were applied, followed by eight types of red base coats. The chemical composition of the various constituents is reported and yielded grouping of the samples into three distinctive classes via PCA and cluster analysis.

Zieba-Palus investigated the variability of the chemical composition of automotive paints across various metallic and plastic body parts [46]. A set originating from 30 different vehicles was analyzed by FTIR and Raman Spectroscopy. Most bumpers consisted of 2-layer systems, while the metallic parts of the vehicles were predominantly 4-layers. Although some metal and plastic parts of the same vehicle contained similar compositions, most samples contained different chemistry identified by FTIR (e.g., binders) and Raman (e.g., organic pigments). Although some differences are expected due to the various functionalities of the body parts, the authors noted that the samples were not guaranteed to be OEM. Therefore, some of the differences may also be due to aftermarket repairs. The study complements existing literature on this topic and reinforces the importance of collecting representative samples near the damaged area to avoid false exclusions during a known-questioned comparison.

Coelho et al. proposed a simplified screening approach to analyze automotive paints by ATR-FTIR as a whole specimen instead of conducting individual layer analyses [47]. The study consisted of fragments collected from six vehicles' hood and side panels. The preliminary findings report notable differences in the various paint sources.

In an article by He et al., ship deck paint was the subject of discrimination studies by ATR-FTIR [48]. The experimental design included 150 ship deck green paints from five brands. From these samples, 125 were randomly used as the training set for the machine learning algorithms, and the remaining 25 samples (5 of each of the five brands) were used for the validation set. The spectra were preprocessed using automatic baseline correction, peak area normalization, multiple scattering correction, and smoothing. Then, three algorithms were evaluated for classification, principal component analysis (PCA), Fisher discriminant analysis (FDA), and K-nearest neighbor analysis (KNN). The classifier algorithms were evaluated in terms of accuracy, precision rate, recall rate, and F-measure. The FDA using the first or second derivative spectra, performed best in correctly classifying the samples by brand and manufacturer (100% correct classification of the validation samples).

In 2020, Wei et al. used chemometric analysis to classify car bumper splinters from hit and runs using ATR-FTIR [49]. Fisher discriminant

analysis (FDA) and support vector machine (SVM) were used to classify 156 car bumper samples from 10 different brands. The classification models were evaluated using the full IR spectra or selected fingerprint regions, with accuracy ranging from 88.5% to 100%, depending on the algorithm employed.

Qiu e al. used data fusion of Micro-laser Raman spectroscopy (MLRM) and ATR-FTIR for characterizing and differentiating 160 bumpers from 8 different manufacturers [50]. Classification algorithms included PCA, Multi-layer perceptron neural network (MLPNN), and FDA. The authors concluded that the fusion spectra models perform better than single spectra datasets, with the FDA with feature-level fusion providing the best discrimination.

Besides IR and Raman Spectroscopy, few studies utilized mass spectrometry methods for paint examinations. In a DART-MS review paper, Sisco and Forbes discuss the existing literature for the application of DART-MS for identifying organic pigments and other organic compounds from paint evidence [51]. In 2022, Gupta and Samal published a review of current DART-MS applications in forensic materials, including paint and tape from improvised explosive devices [52].

In 2021, Alderman et al. investigated Dynamic Headspace GC-MS using activated carbon to analyze volatile organic components in paints and architectural coatings. It was determined that quantitative analysis was feasible for seven distinctive VOCs [53]. In another study, volatile organic components from spray paints were studied by SPE-GC-MS [54]. The headspace above paper sprayed with paint was sampled every 30 min for 4 h using a 65 μm thick polydimethylsiloxane/divinylbenzene SPME fiber and a single quadrupole GC-MS. The study found that VOCs are lost rapidly, but low concentrations remain in the headspace beyond 4 h. Thus, VOCs could be used to establish the time since deposition on a sprayed surface.

1.2.2. Studies related to databases and interpretation of trace evidence

The PQD database continues to be a valuable investigative tool in cases such as hit-and-runs. The database, maintained by the Royal Canadian Mounted Police (RCMP), released an update in 2018 and included a paint search exercise, referred to as a search quiz. The exercise can be used to assess a paint examiner's competence to conduct a PDQ search for training and as a peer-review process to compare consistency in search findings and reporting between analysts and technical reviews. In 2021, Wright published an approach the FBI followed for conducting searches using this quiz tool. She proposed its use for PDQ searches' competency assessment and to establish the required documentation of a technical review [55]. Two analysts conducted the make-model-year searches by the component's text-based system (Layer System Query, LSQ) and spectral library searches using the Bio-Rad® Know-It-All™ software. The article discusses each examiner's independent findings, examples of reporting language utilized at the FBI, and some recommendations.

Klaasse et al. at the Netherlands Forensic Institute presented a prototype multifunctional database, named TraceBase, for forensic trace analysis suitable for investigative and comparative case evaluations [56]. The novelty of the database architecture relies on its capability for data input and output from various trace materials and analytical methods. It is designed as an open-source server-based back-end where a modular approach can retrieve the data. The authors illustrate the utility of the databases with examples for textiles and glass. The database has the flexibility to introduce the data in various formats. For instance, in a textile case, infrared data can be included as full IR spectra, text-based interpretation of IR components, or not be included in the search. The proposed database can potentially facilitate the assessment of the evidential value in comparative studies characterization or identification of unknown samples to provide investigative leads.

The problem of subjectivity in spectral comparisons that heavily relies on human intervention is reported in the comparison of paint and tape for various spectrochemical methods (e.g., comparison of IR, XRF, EDS, Raman). In a recent review paper, Lavine and co-authors discuss the need for statistical support in comparing IR spectra to assess the quality of a spectral comparison and minimize the appearance of personal bias [12]. Quantitative metrics for the comparison of spectra have also been proposed. For instance, Lavine and co-workers and other research groups have broadly reported the statistical comparison of IR spectra of automotive paints for library searching and pattern recognition purposes.

A study by Falardeau et al. addresses the interpretation of paint at the activity level. This study conducted experimental work on the aerosol distributions of fluorescent paint in open and closed environments to evaluate spray paint evidence at the activity level [57]. The surrounding areas were covered with paper sheets, and after spraying, the paper and clothes were observed under regular light and photographed. Luminescence images were also recorded at 450 nm and 570 m and then transformed into black and white images. A computer-based program extracted the droplet features from photographic images to study their size and distribution. For open environments, the authors found some correlations between the droplets' density and the proximity areas that can lead to differentiation of a bystander versus a person performing the graffiti.

Another study addressing the interpretation of paint evidence and other trace materials at the activity level is presented by Letendre et al. [58]. Factors related to background, persistence, transfer, contamination assessment, and activities simulating casework activities and common substrates found at crime scenes were discussed in the manuscript. For paint, the authors gathered information from 134 studies, including population and discrimination studies, background occurrence, and transfer of these traces.

Menżyk et al. discussed the evidential value of polymeric materials using chemometrics and a likelihood ratio approach [59]. The study collected polymeric objects from automotive and household polymer and paint items and analyzed them by NIR and FTIR. Data preprocessing for NIR included standard normal variate transformation (SNV), first derivatives (FD) with a window width of 13 points followed by SNV, and localized standard normal variate transform (LSNV). For FTIR data, the authors utilized the first derivative of the spectra followed by SNV. Likelihood ratios were estimated after dimensionality reduction and feature selection for the probabilistic interpretation of spectral data.

As evidenced from the examples highlighted above, databases, chemometric methods, and more comprehensive interpretation approaches show great potential for better use of the data collected from forensic analyses.

1.2.3. Weathering/stability

The pigment stability during artificial weathering on wood coatings was studied with hyperspectral imaging, reflectance spectrometry, and FTIR [60]. Exposure included cycles of water condensation and UV under controlled weathering conditions for 40 days. The findings indicate that natural indigo was more resistant to degradation than commercial pigments and that the stability is affected by interactions of raw materials. For instance, it was experimentally observed that titanium dioxide accelerated the aging of the paint coatings.

Sanmartín and Pozo-Antonio studied the weathering of graffiti spray paints exposed to UV radiation [61]. The experiment included various surfaces (granite, rhyolite, biocalcarenite, and glass) exposed to long, medium and short UV wavelengths. Thirteen samples were analyzed for each of the four substrates in triplicate, for a total of 208 samples. One sample per group was treated as a control and therefore was not exposed to UV radiation. Analysis by gravimetric measurements, digital imaging, color spectrophotometry, and infrared spectroscopy was conducted at the beginning of the study and four and eight weeks after irradiation. Among the four spray paint colors evaluated (red, black, silver, and blue), only the black paint did not show physical or chemical changes. Short and medium UV radiation caused the most significant physical and chemical changes.

1.2.4. Paint case reports

Kaur et al. present a brief overview of the forensic examination of paints, including a discussion of some cases from the literature [14].

Lee et al. presented a case report investigating three maritime collisions. After a forensic examination of paint residues recovered from the ship of interest, the other vessel(s) involved in two of the three collisions were identified [62]. The samples were taken from various collision sites (e.g., the deck, guardrails, port-side, starboard) and from 2 to 3 suspected ships per case. The analytical scheme included scanning electron microscopy with energy-dispersive X-ray spectroscopy (SEM-EDS), attenuated total reflection–Fourier transform infrared spectroscopy (ATR–FTIR), thermogravimetry (TG), derivative thermogravimetry (DTG), and pyrolysis–gas chromatography/mass spectrometry (Py–GC/MS). The authors presented a detailed description and interpretation of the data and their rationale for their conclusions. This study sets an essential precedent for marine paint examinations and comparisons, which is relatively limited in the literature.

1.2.5. Artwork and cultural heritage

A vast number of paint publications were focused on the authentication of artwork and cultural heritage paint. In a point of view article, Oliviera Andrade discusses the current state and challenges of the forensic analysis of art and cultural heritage items [63]. The authors highlight the need to conduct multidisciplinary and inter-agency collaborations to identify fine counterfeits and alterations, including a vast battery of orthogonal methods.

Sirro et al. utilized Raman spectroscopy on a counterfeit case of fake paintings of the 20th-century Russian avant-garde [64]. The study showed that Raman was sensitive to time markers of the zinc oxide. The results of Raman spectroscopy were complemented with pyrolysis gas chromatography, mass spectrometry, and X-ray analysis. The authors analyzed a collection of over 400 paintings to cover a broad period of dye technology, including the beginning and end of the 20th century (1900–1997). The manuscript describes the basis for differentiating chemical profiles from genuine and fake specimens.

Various analytical tools were presented in the literature for the analysis of artwork and cultural heritage paints, including FTIR [65–70], portable microscopy, and XRF [70,79], SEM-EDS [67,68,70,71], Raman spectroscopy [67,72,73], far-infrared spectroscopy in ATR mode [66], hyperspectral reflectance imaging in the visible [74,75] and near-infrared, XRF [71,76], portable macro X-ray fluorescence [75, 77–79], pyrolysis GC-MS [68,80,81], micro reflectance imaging spectroscopy (micro –RIS) [82] and time-of-flight secondary ion mass spectrometry imaging (TOF-SIMS) [83]. Botteon et al. evaluated the use of portable micro-spatially offset Raman spectroscopy (micro- SORS) to analyze pieces of artwork from the 16th century [84]. Rooney et al. [85] and Taugeron et al. [86] assessed the utility of NMR in studying cultural heritage objects in paint layers.

In 2022, La Nasa et al. used microscopy, SEM-EDS, and pyrolysis GC-MS to characterize the paint components from two Messerschmitt Bf 109 historic airplanes, one from the *Deutsches Museum* collection and one privately owned [81]. Depending on the area of the plane, 2 to 13 layers were fully characterized and attributed to the first factory paint, the Legion Condor, Spanish Airforce, or museum preservation paints. This is the first study of this kind reporting the characterization of original aircraft paint materials fabricated in the 1920s and repainted during various subsequent periods.

In the same year, Tutt and Hoffmann presented an interesting approach to the forensic examination of historic vehicles, an area of forgery that is recently growing due to the increased market value of these collection automobiles [87]. A multi-technique and interdisciplinary approach was utilized to illustrate various case examples.

1.2.6. New trends in paint formulations

Nanomaterials are becoming more prominent in paint formulations in automotive, marine, and other industrial applications because their mechanical, thermal, electrical, chemical, and physical properties favor the robotic nanospray painting process and overall end-product quality [88–93]. The automated spray painting is most common on the anti-chip coat, primer surface, base coat, and clear coats, although they are applicable to other paint layers. Several studies discuss the use of paint infused with carbon nanotubes (multiwall carbon nanotubes, WWCNTs) by ultrasonication and magnetic stirring processes to enhance the quality of spray coating [94,95]. Modifications of carbon nanotubes (CNTs) and epoxy-CNT composites have also been investigated [93,96]. The MWCNTs are rolls of graphene produced by chemical vapor deposition, often in polyurethane base coats. Typical sizes range from 30 to 80 nm in diameter and are 5 μm long [95]. Advantages of the nano paints are the improved quality, including anti-corrosion, self-cleaning, coolant/isolating properties, smoother surfaces, and increased life span. Also, they provide a more environmentally friendly and cost-effective approach. As a result, they are anticipated to become more commonly observed in casework items. These nanomaterials have been analyzed by Raman spectroscopy, XRD, SEM-EDS, Transmission Electron Microscopy TEM, and Differential Thermogravimetry DTG, to mention some [95, 97].

Advances in anti-corrosion coatings have gained attention recently, as many corrosion protection systems are based on chromates and volatile organics that are no longer environmentally sustainable. Graphene has been used for the cathodic protection of zinc-rich epoxy coatings [98,99].

Sukanya et al. reviewed the state on the development of anticorrosive films other than graphene, including layer double hydroxides (LDHs), transition metal dichalcogenides (TMDs), MXenes, layered hexagonal boron nitride (h-BN), and graphitic carbon nitride (g-C3N4) [100]. The LDHs are species that contain divalent or trivalent cations such as Mg^{2+}, Zn^{2+}, Fe^{2+} or Ni^{2+}, Al^{3+} or Fe^{3+} and cations such as carbonates, chlorine, sulfates, and RCO_2^-. The TMDs, are often represented as MX_2, where M is a transition metal such as Mo or W, and X represents atoms such as S, Se, or Te. The MXenes are another emerging family of coating materials comprised of metal carbides or nitrides (e.g., $Ti_3C_2T_x$). The MXenes nanosheets have a large surface area with a surface chemistry that favors mechanical properties with good thermal and electrical conductivity. The MXenes can be functionalized with binders such as epoxy and silane. Finally, graphitic carbon nitride (g-C3N4) and h-BN are analogous to graphene in terms of mechanical, thermal, hydrophobic, and permeability properties and prevent the diffusion of corrosive analytes. These can also be functionalized with epoxy and polyurethanes and combined with iron oxide nanoparticles (Fe_3O_4) to enhance the corrosion-protective coatings.

Research continues on the development of eco-friendly solvent-free powder coatings. Li et al. reported using waterborne epoxy coatings with functionalized nanomaterials [101]. For this purpose, MXene-packed structure nanosheets were modified with L-Cysteine to favor anticorrosion and weather protection. The coatings were analyzed by FTIR, XRD, EDS, and XPS, and the anticorrosion properties were measured via electrochemical methods. Wang et al. evaluated silanized Mxene/-carbon nanotube composites to aid anticorrosion of polyurethane coatings [102]. The carbon nanotubes and the functionalized surfaces of $Ti_3C_2T_x$ and S-CNTs form a shield layer that prevents penetration of corrosive analytes.

New technological advances have also made possible the use of powder coating in non-metallic surfaces, such as medium density fiberboard (MDF) [103], using low-temperature curing processes. The coatings are created with polyester-hybrid technology with a complete binder package that adheres to MDF and metal with film thicknesses of up to 125 μm per application.

Significant advances for automatic repairing of defects have been made in the last decade within novel self-healing polymeric materials. Hong et al. developed a disulfide polyurethane diol adduct (DSPUDA) with reversibility of bond cleavages that promotes the auto repair of scratches [104]. Nano-scratch tester and an atomic force microscope are

among the instrumentation utilized in this study. Cui et al. also investigated novel scratch resistance and self-healing automotive clear coatings using polymer/graphene composites [105]. Zotiadis et al. reported successful repairing of microcracks on alkyd-based coatings using epoxy microcapsules loaded with poly urea-formaldehyde [106].

Another area of interest in coatings technology is the development of UV curable powder coatings. Czachor-Jadaka et al. reviewed the advances in UV curable powder coatings and their advantages compared to thermally cured coatings [107]. A detailed discussion of the literature on the chemical structure of resins is presented in this review, including unsaturated photoinitiators and additives used in the formulation of UV-curable polyester, urethane acrylates, acrylate and methacrylate resins, epoxy, and polyamides.

The global market of metallic pigments is growing and driving innovative formulations. It is expected to reach $1.20 billion by 2022 [108]. Among the leading pigments, aluminum and copper pigments account for one-third of the total market, including newer technologies compatible with lower solvent carriers and waterborne coatings. Current trends for more sustainable paint industries are driving away from lead chromate and other leaded pigments.

The automotive refinish coatings market is also following innovations pushed by greener options, with polyurethanes and acrylic latex waterborne basecoat technology being the most popular in collision repair centers [109]. Primer aerosol coating technology that cures by UV lamp in a few minutes has also been introduced in the auto refinish market.

Thejo Kalyani et al. reviewed luminescent paints' scientific foundations and applications [110]. Although this type of paint is not commonly encountered in casework, forensic examiners may find helpful information in this article as the number of applications is numerous, and the likelihood of occurrence in particular cases may increase in the future. Among the many uses of luminous paints and pigments, the authors described persistent paints used in roads, building signs, construction materials to visualize materials failures, clocks, lamps, biosensors, forgery identification, and anti-counterfeiting. In the March 2022 volume of the Coatings World Magazine, PPG announced the launch of the first-of-a-kind retroreflective coating (Envirocron LUM powder coating) for a variety of applications, including bicycles, scooters, safety equipment, tools, fences, shopping carts, and road guardrails and signs.

Recycling in the paint industry is also part of global sustainability projects. To minimize the environmental footprint of automotive paint waste, a group in Malaysia evaluated the feasibility of recycling paint sludge disposal to create concrete products [111]. From a forensic point of view, these recycled materials must be on the lookout for forensic practitioners.

The architectural coatings industry has also changed its formulations over the last decade. One of the most notable is the shift from oil/solvent-based to waterborne paints [3,112]. Environmental regulations have also influenced VOC reduction in latex-based waterborne coatings. As a result, zero-VOC coalescents have been developed, and resins have been adapted to require little to no solvent to form the film. Various paint manufacturers incorporated different low and zero-VOC products into the market. Surfactants like alkylphenol ethoxylates have been banned in Europe and are encouraged to be replaced in some areas in North America due to concerns of bioaccumulation in the environment. Therefore, alternative APE-free resins and surfactants are being used in architectural paints. Alternative surfactants of particle size smaller than 200 nm are required to maintain the stability of these APE-free formulations. Pyrithione compounds and various zinc, silver, or copper preservatives have replaced organic solvents and formaldehyde-containing preservatives. Another critical transition in architectural coatings is the paint-and-primer-in-one products which provide faster applications for the end-users. This has required using pigments with higher hiding power like pigment red 254 or pigment yellow, or dispersing agents that distribute the titanium dioxide in the dried film better.

1.3. Tape evidence

Among the many types of tapes recovered at crime scenes and examined at forensic laboratories, the most popular are electrical, duct, and packaging tape. These materials are often used to bind or gag victims in kidnappings, sexual assaults, and homicides. Also, they are employed in the fabrication of improvised explosives devices, the packaging of drugs, and the sealing of objects involved in criminal activities. Therefore, the physical and chemical examination of pressure-sensitive tapes can provide valuable investigative and intelligence leads and assist the trier of fact with their decisions. Moreover, tape evidence is prone to trap other traces that can become relevant during an investigation, such as DNA, hairs, fibers, fingerprints, and drugs or explosives residues, to mention some. Thus, some studies have focused on how to preserve and recover those traces.

From 2020 to 2022, the forensic examinations of tape have gained attention in various areas, such as the assessment of emerging methods, evaluation of error rates of conventional analytical protocols, statistical interpretation approaches, and evidence preservation. The following sections discuss the most recent literature on these subjects. However, since this is the first time that tape has been incorporated in the INTERPOL reviews, we have included some older pertinent literature.

1.3.1. Emerging analytical methods

Most of the research on emerging analytical methods was focused on electrical and packaging tapes, rather than duct tapes, possibly due to the more significant amount of distinctive physical features observed in the latter. The analytical methods for improved characterization and interpretation of tape evidence reported in this review have been centered on spectroscopic and mass spectrometry techniques.

Characterization and analysis of organic compounds have been reported by infrared spectroscopy (FTIR, ambient ionization methods, and mass spectrometry). Infrared spectroscopy has been long used as a primary tool for the classification and comparison of tapes, and newer studies increase this body of knowledge with a particular emphasis on data analysis and chemometrics. Zięba-Palus utilized infrared spectroscopy for the classification and comparative analysis of packaging, insulation, and duct tapes of various colors [113]. In this study, the backing and adhesive of 50 samples were investigated by FTIR operated in transmitted mode. Although previous studies have demonstrated the utility of FTIR in the laboratory analytical workflow [23,114–116], this manuscript provided helpful insights into the identification of chemical components. Backings were separated by polymer type into four major groups, with some samples further discriminated based on the spectral comparison in two of those groups. Adhesives were clustered in five groups based on the presence of isoprene rubber, styrene-butadiene rubber, esters, or acrylates. Some discrimination was observed for tapes belonging to the same subgroup by their relative amounts of styrene, carbonates, titanium dioxide, kaolin, and compounds containing a carbonyl group.

In 2022, Nimi et al. examined 75 tape samples originating from 25 brands of electrical tapes by ATR-FTIR [117]. Data reduction and classification methods (principal component analysis, PCA and linear discriminant analysis, PCA-LDA) were used to group samples based on their spectra. Correct classification rates ranged from 80 to 89% for the adhesive and 84–100% for the backing side. Also, the potential interference from substrates like cardboard, glass, plastic, and steel was investigated and showed that background contaminations influenced the accuracy of adhesive while the backing spectra remained unaltered.

In a study by Oliva et al., laser-assisted sampling (LAS) and direct desorption flowing atmospheric-pressure afterglow mass spectrometry (LAS-FAPA-MS and FAPA-MS) were evaluated for tape analyses [118]. The authors indicated that the advantages of LAS-FAPA-MS compared to regular Pyrolysis GC-MS are the minimal sample preparation, real-time

analysis, and higher degree of spatial information. The ambient ionization apparatus was coupled to a high-resolution mass spectrometer (LTQ- Orbitrap XL) and operated in positive ion mode. In this study, the backing and adhesive layers of 15 masking, electrical, and duct tapes were analyzed, and their mass spectra were compared for classification and comparison purposes. Direct desorption-FAPA-MS provided information on the surface's polymer additives, while LAS-FAPA-MS complemented the spectral data with higher *m/z* peaks and more fragmentation. The identification of the *m/z* fragments for 21 compounds is thoroughly discussed in the manuscript, providing a valuable body of foundation for the compound characterizations. The principal component analysis of the combined spectral data showed discrimination capabilities ranging from 80 to 100%, depending on the tape type.

Zhang et al. investigated the use of a diode laser-assisted micro-pyrolysis program (LAMP) coupled with flowing atmospheric-pressure afterglow ambient mass spectrometry (FAPA) for the direct characterization of polymers and polymer additives [119]. The method was effective in desorbing, pyrolyzing, and ionizing polymer species and their additives. Pyrolysis products were observed in positive and negative modes and confirmed with high-resolution mass spectrometry. Advantages of LAMP compared to regular pyrolysis are superior throughput, faster temperature control, analysis in real-time, and MS imaging with high spatial resolution.

The application of high-resolution magic angle spinning (HR-MAS) 1H NMR spectroscopy was evaluated for tapes [120]. The results for 90 black electrical tapes were compared to those obtained by the FBI after following their typical analytical scheme (microscopy, FTIR, SEM-EDS, and Py-GCMS. One advantage of HR-MAS is that it is suitable for insoluble materials if they are swellable. The sample preparation consisted of placing approximately 10 mg of the tape in a 4-mm ZrO2 rotor and filling it up with about 70 µL CDCl3. The data was analyzed using hierarchical clustering (HCA). The performance of HR-MAS was superior to conventional methods (98.4% for HR-MAS vs. 96% for all other techniques combined).

Besides the characterization of organic constituents, several studies focused on improved methods for inorganic analysis. The value of elemental analysis of tapes by SEM-EDS has been previously reported in the literature and widely adopted in the field [23,116]. Additional research explored alternative elemental techniques that can achieve higher discrimination and complement conventional analytical schemes, namely X-ray Fluorescence Spectroscopy (XRF) [121,122] and Laser-Based methods such as Laser Ablation Inductively Coupled Plasma Mass Spectrometry (LA-ICP-MS and Laser-Induced Breakdown Spectroscopy (LIBS) [123–126].

The elemental analysis of electrical tape by X-ray Fluorescence (XRF) has demonstrated its forensic utility for classifying unknowns and comparing known and questioned tapes. In a study by Prusinowski et al., three XRF systems were used to evaluate a range of configurations typically used at forensic laboratories [121]. The discrimination for a set of 40 electrical tapes manufactured from various sources and grades increased from 78.8% by SEM-EDS to 84.6% by LA-ICP-MS and 81.5–91.0% by XRF for 150um spot size iXRF with SiLi, 25 µm spot size benchtop XRF with SD detector, and 1 cm spot size XRF with SiLi detector, respectively. No false exclusions were observed in an additional dataset of 20 fragments of tape originating from the same roll and measured in various replicates on the same and different days.

In a follow-up study by Brooks et al., 114 electrical tape backings originating from 94 different samples and 20 items from the same roll were used as part of the method validation [122]. Improved classification capabilities were observed for XRF over SEM-EDS, as shown by its ability to detect more elements (14 vs. 6) and distinguish the samples into a larger number of groups (61 distinctive groups vs. 15). The superior performance for characterizing elemental profiles also improved discrimination power (96.7% u-XRF vs. 87.3% SEM-EDS). Also, the performance, advantages, and limitations of different spectral comparison methods are reported in this study, such as spectral overlay, spectral contrast angle ratios, and Quadratic Discriminant Analysis (QDA).

Martinez et al. reported a series of four studies [124–126] that demonstrated the powerful capabilities of LA-ICP-MS for identifying major and minor elements on tapes and using their elemental profiles for investigative leads and source comparisons. In the first study, the backings of 90 black electrical tapes were analyzed by LA-ICP-MS [123]. The results were compared to a typical analytical scheme for tape examinations (microscopical examination, Scanning Electron Microscopy-Energy Dispersive Spectroscopy (SEM-EDS), Fourier Transform Infrared Spectroscopy (FTIR), and Pyrolysis–Gas Chromatography-Mass Spectrometry (Py–GC–MS)). The study demonstrated that LA-ICP-MS alone captured a vast amount of chemical information of the formulation components and resulted in improved discrimination and superior characterization compared to the combined analytical protocols. The results suggested that LA-ICP-MS has the potential to be adopted at the front of the analytical workflow for fast decision-making and informative leads. The LA-ICP-MS method alone provided 94% correct discrimination of the tapes known to originate from different rolls and 100% correct association of the tapes known to originate from the same roll.

The second study expanded the application of LA-ICP-MS and LIBS to packaging tape. The methods allowed the characterization of ten relevant elements by LA-ICP-MS and seven by LIBS, including lithium, potassium, and sodium, which LA-ICP-MS did not easily detect [124]. The selected elements demonstrated good reproducibility within a single source and good discrimination between different sources. The LIBS and LA-ICP-MS data provided some orthogonality, with added discrimination when combined.

In the third study, the LIBS and LA-ICP-MS protocols were subject to two interlaboratory exercises in an effort toward method standardization [125]. Seven laboratories participated in the exercises, which evaluated the capabilities of SEM-EDS, LIBS, and LA-ICP-MS for the forensic comparison of electrical tapes in mock cases that compared known versus questioned items. The results show good agreement among the participants when using the same analytical instrumentation. All the laboratories conducting SEM-EDS, LIBS, and LA-ICP-MS correctly associate the K-Q pairs of tapes originating from the same rolls (no false negatives reported). False positive rates ranged from 13% to 17% by SEM-EDS, depending on the exercise, while no false positives were reported by any of the LIBS and LA-ICP-MS participating laboratories. The increased discrimination observed by the laser-based methods results from the superior sensitivity and selectivity of the methods. For instance, in this dataset, SEM-EDS detected up to seven elements in the samples of interest, while LIBS and LA-ICP-MS characterized up to 17 and 32 elements, respectively.

Finally, the fourth study presented by this research group uses likelihood ratios to assess the probative value of tape evidence [126]. The authors conducted data reduction of the LA-ICP-MS spectra by PCA, then used scores of the first five principal components as input to estimate the LR. A posthoc calibration assisted in yielding log LR in more realistic ranges per the dataset size. Low false inclusion and false exclusion error rates of 3.7% and 2.2% were reported, demonstrating the utility of the proposed approach to assess the weight of high-dimensional data.

Kuczelinis et al. developed and characterized a polymer-based in-house calibration standard for examining electrical tapes by LA-ICP-MS [127]. A collection of 87 PVC black electrical tapes from different rolls were analyzed using a semiquantitative method to characterize up to 30 elements in the backings. In addition, a same-source set of 24 samples (3 fragments from 8 sections) from each of three different rolls was evaluated for false exclusions. The selected match criteria yielded less than 0.7% false exclusions and less than 2.5% false inclusions. In another study by the same team, a novel method was developed using picoliter-volume standard addition to quantify elements in polymeric materials by LA-ICP-MS [128].

These studies suggest that forensic laboratories can benefit from shifting from SEM-EDS to more sensitive methods (u-XRF, LIBS, or LA-

ICP-MS) for the forensic characterization and comparison of electrical tapes.

1.3.2. Physical fits of tape materials

Regardless of the general probative value assigned to physical fits (a.k.a. fracture match), standard criteria and protocols to determine what constitutes a match are still in the early development stages. As a result, we observed a trend in the physical fit literature toward demonstrating the scientific foundations of fracture fit examinations. Various approaches were developed to mitigate bias and assess the relevance of the evidence.

Brooks et al. review the current state of physical fit research in trace evidence materials [129]. The manuscript discusses the foundations and limitations of the discipline for casework protocols and case reports, fractography and qualitative-based studies, and quantitative assessments of physical fits.

Recent studies formally evaluate the incidence of error rates and accuracy in determining matches and non-matches of fractured trace materials. The reported datasets range between 30 and 2200 samples, evaluated by single or multiple analysts.

A group at the University of California at Davis conducted pioneer research in the quantitative assessment of duct tape physical fits [130]. The authors studied four different types of separation methods (hand--torn, Elmendorf torn, scissor cut, and cutter cut) on over 2000 duct tape pairs of varying grades and colors. A first effort to provide a quantitative measure of the quality of the match was calculated using a match score as the relative "matching length" divided by the overall width of the tape. Statistical analysis was focused on reporting performance rates. The dataset produced mean accuracy ranging from 98 to 100% for torn tape and 98–99.8% for cut tape. False-positive rates lower than 0.7% and 3.3%, and false-negative rates lower than 2.7% and 0.3% were reported for hand-torn and cut-tapes, respectively.

In 2020, Prusinowski et al. developed a systematic method to quantify the quality of a duct tape physical fit using a similarity score named Edge Similarity Score (ESS) [131]. The ESS uses the duct tape scrim bins as the smallest comparison unit in a reproducible manner. Then, the ESS is estimated as the relative percent of scrim areas across a questioned fractured edge that "fit" the known comparison tape. This simple approach provides a quantitative estimation of a fit's quality while assuring that the peer-review process can be conducted in a systematic, transparent, and reproducible fashion. Performance rates were estimated for a blind dataset of over 2200 tapes, including sensitivity, selectivity, and accuracy. The effects of the separation method (cut vs. hand-torn), stretching, and tape grade (low, medium, and high grade) on ESS distribution are reported. The study demonstrated that accuracy from 84.9% (higher quality hand-torn set) to over 99% (low and mid-quality sets) is feasible, with no false positives reported. Moreover, the ESS score can be used as a metric to inform and support the examiner's decision. Score likelihood ratios were used as a proxy for the weight of the evidence. Relative scores served as a good predictor for fracture match determinations and provided a means for statistical support for the examination of fracture fits. ESS higher than 80% provided a score likelihood ratio (SLR) that supported the conclusion of a match, and ESS lower than 25% provided an SLR supporting the decision of a non-match.

Another interesting approach to assessing the evidential value of duct tape physical fits was presented by van Dijk et al. [132]. Here, the authors developed a novel method using likelihood ratios and Bayesian networks to evaluate the weight of the evidence. The study focused on duct tapes with weft-insert patterns, consisting of weft fibers inserted into the gaps between the chain-like warp loops. Briefly, 136 pieces of various duct tape grades were separated by three people, using either a tearing from top-down or bottom-up, creating 272 edges, with a total of 127 true fit pairs. Various BN models were used to estimate the probabilities under the competing hypothesis, Hp and Hd. One of the assumptions made for the models is that the loop breaking patterns comply with the Markov property, where the state of a loop is assumed to only depends on the state of the loop above it. The probability estimates were based on data from the features imparted on the broken loops on torn ends, theoretical input, and expert knowledge. The performance of likelihood ratios was assessed using ECE plots and demonstrated that the system was well-calibrated. Also, this study presented a proof of principle to address the question of how the value of the evidence is influenced by the presence of a partially fractured edge.

1.3.3. Interpretation of tape evidence and tape as substrate for other traces

Weiten et al. presented an interesting discussion of the application of Bayesian Networks to interpret traces left behind on tape surfaces at the source and activity level [133]. Fingermarks and biological fluids were evaluated at the source level. Then, activity factors were considered in their interpretation models, such as recovery, transfer, persistence, and estimation of the position of the sampling location on the original roll based on fracture fits.

A case study involving the use of duct tape, fingermarks, and DNA was used by de Koeijer et al. to illustrate a practical interpretation approach using Bayesian Networks to combine different evidence types of evidence and explain their combined strength to the courtroom [134].

Tape lifting has also been proposed as a forensic approach to recovering particulates and traces that offers the benefits of being cost-effective and creating a secure environment for the residues of interest [135–139]. Gwinnett et al. reported using tape (Easylift) for lifting and monitoring micro polymers [140]. The study reported that in situ analyses of microplastics and fibers were possible through the adhesive since it was compatible with polarized light microscopy (PLM), confocal Raman spectroscopy, fluorescence microscopy, microspectrophotometry (MSP), and hyperspectral microscopy. Kanokwongnuwut et al. evaluated 14 tapes to recover and visualize cellular material using DD staining and fluorescence microscopy [141]. Three types of tapes showed utility in the collection and screening of touch-DNA, as they did not inhibit direct STR amplification or masked the fluorescence examinations.

In 2020, Chadwick and all performed an extensive study to evaluate if chemicals used to enhance fingermarks negatively impact the physical, optical, and chemical comparative analysis of duct tape evidence [136]. Untreated tapes were compared with those treated with fingermark enhancers, namely cyanoacrylate, cyanoacrylate stained with rhodamine 6G, and Wet Powder™. Physical and optical examinations were conducted on a stereomicroscope and Video Spectral Comparator (VSC), while chemical analyses were done via ATR-FTIR. Compared to cyanoacrylate-based chemicals, wet powder suspensions were more suitable as they did not affect the physical and chemical characterization of the tape adhesive or backings. The results demonstrate that the applied chemicals had minimal impact on most of the physical or optical characteristics of the tapes selected. Still, differences in the infrared spectra can lead to misidentifications. However, the authors propose an operational workflow that can help forensic examiners to determine the type of developing treatment performed on a tape and use this information during the interpretation of the data rather than evaluate the results in isolation.

1.4. Glass evidence

1.4.1. Industry data, forensic laboratory management, book chapters and review papers

The annual sourcebook for the glass industry, published in July 2022 by the National Glass Association (NGA), contains a list with contact information to over 1200 companies in more than 700 product categories including glass manufacturers, distributors, and suppliers; https://www.glassmagazine.com/issue/july-2022. The NGA forecasted continued growth in glass production for developed economies, in particular for the U.S. float glass industry with expected growth between 20 and 45% from 2018 to 2022 despite the challenges posed by the

pandemic. A downloadable global float plant database that includes dozens of different float glass manufacturers operating more than 230 plant locations with more than 450 float glass lines is available from NGA. The World of Glass 2021 Report [142] lists notable expansion in glass manufacturing in the U.S. including four new float lines in North America.

The Project FORESIGHT Annual Report for 2020–2021 (published in May 2022) [143] is a business-guided self-evaluation of forensic science laboratories around the globe, with more than 190 laboratories providing data. The report includes metrics to assist forensic science managers evaluate work processes and laboratory productivity. The aggregate productivity for trace evidence sections, including all materials analyses (e.g. paint, tape, glass and fiber evidence but not fire debris analysis) is reported for casework submissions from July 1, 2020 to June 30, 2021. Some important takeaways from the report include that trace evidence cases include more "items", "samples" and "tests" than almost every other evidence type submitted to the laboratory. The median number of trace evidence "tests" performed per 100,000 population served in a locality is reported as ~27 "tests", in comparison to ~828 "tests" for DNA casework/100,000 population and ~1500 Drugs-Controlled Substances/100,000 population. The median "cost" for the average trace evidence case is reported as ~ $ 5000. in comparison to ~ $ 3700/case for DNA casework and ~ $ 400./case for drugs-controlled substances casework. The complexity of a trace evidence "case" results in a more expensive examination that is less requested in a locality.

A very basic overview of paint, soil and glass evidence was published as a chapter in a recent book [144]. While this chapter does not report anything new to add to the literature, it does explain the use of these types of evidence in a forensic laboratory. A different, similarly introductory chapter on glass analysis was published in another book [145] and a third chapter, also introductory in nature was published in a different book [146]. A more comprehensive and advanced chapter in another book [147] includes more up-to-date information on glass analysis and interpretation with an emphasis on the interpretation of glass evidence using recently reported methods.

Two different laboratory experiments were published in a teaching laboratory manual. One set of experiments featured glass breakage determinations [148] and one set of experiments featured glass examinations [149].

An excellent recent review of the literature [11] focuses more generally on the scientific foundations of trace evidence analysis. The review provides information on manufacturing, physical and chemical analysis, transfer and persistence and recent trends in the interpretation of trace materials evidence. In addition to paint, tape, and glass evidence, this very thorough review, consisting of more than 450 references, also includes sections on hair and fiber evidence examinations.

1.4.2. Physical and optical measurements and examinations

A study that examined the glass fracture patterns/characteristics after a shotgun blast to different types of glass (e.g. soda-lime and tempered glass) of different thicknesses and at different distances from the shotgun to determine hole diameters and "dicing" resulting from tempered glass, a not surprising observation [150].

Another study [151] evaluating the bullet hole morphologies in glass to associate distance from firing, projectile type, speed and angle of entry was also published. The authors aim to improve crime scene reconstruction events based on a better understanding of the morphological features of the bullet holes.

Haag and Haag [152] also describe bullet interactions with glass in order to better understand the nature of glass particles imbedded in recovered bullets to differentiate glass-imbedding from other silica-containing minerals such as sand and quartz primarily by polarized light microscopy.

A thesis by Beach [153] describes how a projectile impact on glass can result in different types of fracture patterns. The study includes how variations of glass type, glass thickness, curvature, distance from a firearm muzzle, contact angle, and the type of projectile can correlate to fracture patterns on the glass. The study also aims to correlate impact energy to the degree of glass fracture including the impact of muzzle-to-target distance for different firearm and ammunition combinations and including the use of a Doppler radar system to measure the projectile velocity.

Dondeti and Tippur [154] describe failure behavior and fracture mechanics of hairline cracks in glass due to stress sites. The authors evaluate crack initiation and quasi-static crack growth from a self-healed crack in soda-lime glass plate by calculating the stress intensity factor (SIF) history for the stress event.

Jiang et al. [155] aimed to better understand the dynamic tensile characteristics of glass by investigating the effects of loading rate, glass size and stress waves on the dynamic tensile behavior of brittle glass. Dynamic flexural stresses were induced with stress pulses and the tensile characteristics were viewed by high-speed photography. The authors report that the dynamic tensile stresses within a glass specimen reached a maximum at the same time as a crack starts.

Grant et al. [156] used attenuated total reflectance Fourier transform infrared (ATR-FTIR) to examine automotive window tints and then applied chemometric tools to differentiate the polymer types of different tint products. The authors report being able to associate unknown tint samples to a known brand.

Viviani et al. [157] evaluated the effects of explosions on laminated glass plates constructed from glass panes bonded by thin polymeric interlayers, in the pre-glass-breakage phase. The authors describe the viscoelastic properties of the interlayer and thereby producing a model of the coupling between the glass and the polymer laminate that can assist with future design of laminated glass.

Voros et al. [158] further examined the effect of annealing on the refractive index of glass that was subjected to heat such as in a house fire. The authors collected toughened non-toughened glass microfragments and simulated exposure to a fire by heating the glass in a furnace for various times at 450 and 650° C and cooling down quickly to model different heat expositions. The authors report a significant change in the RIs in all cases. However, after annealing the samples from the same source were associated and samples from different sources were discriminated by RI as previously reported by others.

Podor et al. [159] directly observed the formation of crystals in glasses, phase separation, chemical reactivity or glass foaming directly by use of an Environmental Scanning Electron Microscope (ESEM) equipped with a high temperature furnace. These observations can lead to a better understanding of how heat can impact the physical and optical properties of glass.

A study by Nentwig et al. [160] assessed the medical and biomedical impact from blows to a human head using different glass bottles to evaluate the injuries to facial and cranial bones resulting from the impacts. The authors concluded that blows with a 0.5-l beer bottle or with a 0.33-l Coke bottle to the head can transfer up to 1.255 N of force and thus are able to cause severe blunt as well as sharp trauma injuries.

Brooks et al. [129] conducted a thorough review of the literature on physical fit determinations, including work on tape, textiles, and polymers but also glass. The authors focused on case reports, fractography studies, and quantitative assessment of a fracture fit. The authors note a recent shift in research that focuses on quantitative, performance-based assessment of error rates associated with physical fit examinations and with the application of likelihood ratios to determine evidential significance. The authors also include reports of probabilistic interpretations of large sample sets and the implementation of automatic edge-detection algorithms to support expert opinions.

Thompson et al. [161] report on the development of a computational framework that uses fracture mechanics and statistical analysis to provide a quantitative match analysis for match probability and including error rates for the match analysis. The framework employs the statistics of fracture surfaces at microscopic scale, defined as greater than two

grain-size or micro-feature-size, and assumes that a fragment "have the premise of uniqueness which quantitatively describes the microscopic features on the fracture surface for forensic comparisons". The methods used include 3D spectral analysis of overlapping topological images of the fracture surface to classify specimens using statistical learning and matrix-variate models. A set of thirty-eight different fracture surfaces of *steel* articles were correctly classified. The authors claim that this framework lays the foundations for forensic applications with quantitative statistical comparison across a broad range of fractured materials with diverse textures and mechanical properties.

Voros et al. [162] simulated a case involving refractive index measurements of very small (250 μm) fragments recovered from garments after breaking a pane of float glass. Refractive index was measured for fragments that were crushed and not crushed. The authors note some non-matches for surface fragments of non-crushed samples. The authors conclude that crushing improves the probability of "matching" and improves the edge count values during the RI measurement.

Voros et al. [163] also report on the value of annealing glass that has been subjected to thermal stress before measurement of the refractive index, as previously reported by others. The experiments were carried out on fragments in the range of ~100 μm.

1.4.3. Chemical measurements

Ernst et al. proposed an approach to compare ceramic frit in vehicle windows by XRF [164]. The authors investigated the discrimination of ceramic frits from twenty-five vehicle windows by physical observations, microscopy, and micro-X-ray fluorescence (XRF). The set included twelve windshield panes, eight rear windows, four side windows, and one sunroof obtained from 22 different vehicles manufactured from 2002 to 2016. Three XRF instruments with different configurations were utilized to evaluate the elemental profiles, including mono and poly-capillary systems equipped with SiLi or SD detectors. The XRF yielded discrimination ranging from 97 to 100%, depending on the instrument and match criterion utilized.

Cagon et al. [165] compares the performance of four non-destructive techniques for in situ characterization of leaded glass windows. Macroscopic X-ray fluorescence imaging (MA-XRF), UV–Vis–NIR, Raman spectroscopy, and infrared thermography (IRT) are used to assess the ability of these techniques to group colorless glass panes based on differences in composition. IRT, MA-XRF and UV–Vis–NIR spectroscopy was able to distinguish at least two glass groups with MA-XRF providing the most detailed chemical information, not surprisingly. Potasium (K) and calcium (Ca) were used along with decolorizers (Fe, Mn, As) to further group glass samples. In addition, UV–Vis–NIR detected cobalt and iron where Raman spectroscopy was reported as hampered by fluorescence caused by the metal ions of the decolorizer in most of the panes but nevertheless was able to identify one group.

Wimpenny et al. [166] report on a study focused on the chemical and isotopic compositions of major and trace elements and their relationship within a population of fallout samples resulting from a nuclear test event. The authors aim to better understand how fallout melt glass formation in near surface environments is influenced by that environment and demonstrate how major and trace element abundances can provide useful insights into chemical processes within the fireball post event. Isotopically enriched uranium (presumably from the weapon) and natural composition uranium (from a combination of anthropogenic and environmental materials from within the blast zone) were detected. The association of the composition of local soils from the event site suggest that local soils are the most probable source of entrained material into the fireball and the source of material into which the bomb vapor was incorporated. Processes such as condensation from the fireball were modeled to better understand the composition of macroscale fallout melt glass.

Jacquemin et al. [167] report on the use of Raman imaging to investigate the homogeneity of the Raman response at the surface of casted aluminosilicate glass pieces. Samples were probed at constant focus depth across 7 × 7 cm^2 surfaces using 500 μm spatial steps, resulting in large and detailed Raman images. The authors show that the modification of the Raman response is small across the scanned area and that the information is carried by the spatial representation of the selected Raman parameters, in particular the Si–O stretching mode involving Q2 tetrahedral units, and the Si–O–Si bending vibrations envelope in the low-wavenumber range were of interest. The evolution of Raman parameters across the surface of the sample permitted the identification of areas consisting of material from different stages of casting. The authors report the ability to observe structural and chemical changes originating from the manufacturing process of the glass pieces as revealed by Raman imaging.

Merk et al. [168] used laser induced breakdown spectroscopy (LIBS) and Raman, in combination, to discriminate sixteen different glass samples by use of principal component analysis (PCA). The LIBS/Raman results were compared to μ-XRF and SEM-EDS in this work. The authors report very good discrimination (up to 99%) when LIBS and Raman are used jointly. The authors only report the source of the Raman signals as "fluorescence" but do report the use of trace elements (e.g., Fe, Ti, Ba, Sr) for discrimination purposes.

Corzo and Steel [169] reported on the use of micro X-ray fluorescence spectrometry (microXRF) for the analysis of small (<1 mm) glass fragments that are partially transparent to the X-ray beam with an aim to better understand the signal-to-noise ratio (SNR) of the determination. The authors note that, in addition to fluorescence, the primary beam X-rays may scatter within the chamber and provide noise in the measurements. The fragments were mounted on a 3D-printed plastic mount to allow fragments to be raised as high as possible from the sample stage, thereby minimizing stage scatter and improving the SNR for most elements with the greatest improvement (>30%) observed for the lower atomic number elements (Na and Mg) and higher atomic number elements (Sr and Zr). An additional simple method to improve SNR was the use of primary beam filters with elements containing characteristic lines in the high-energy range (Rb, Sr, and Zr) showing the greatest improvement (>70%) in SNR.

Samanta et al. [170] utilized Instrumental Neutron Activation Analysis (INAA) for multi-elemental analysis of soda-lime glasses. Five automobile glass fragments were analyzed by INAA targeting seven trace elements of interest. Concentrations of Sc and elemental concentration ratios such as La/Sc indicated that five glasses fall into two major groups, which was confirmed by statistical cluster analysis.

Kaspi et al. [171] report on the use of particle-induced X-ray emission (PIXE) for elemental analysis of glass fragments. The authors claim that the use of a PIXE workflow, in combination with machine learning (ML) can "produce models with better than 80% accuracy in identifying glass" sources but the study fails to describe the underlying analytical figures of merit for the PIXE method such as bias, precision and limits of detection for the list of elements reported. The authors also fail to compare the PIXE performance to existing, more routinely used techniques for which analytical standard methods of analysis already exist (e.g. micro-XRF, solution ICP-MS and LA-ICP-MS).

A follow-on paper by the same group [172] reports on the "classification" of glass from car windows from different cars using PIXE as well as "possible glass corrosion". The authors claim to have developed a database for use in a classification model. The authors do not address the practical aspects of maintaining proton-ion beam PIXE instrument in a typical forensic laboratory and do not report the analytical figures of merit for PIXE on standard reference materials, for example, in order to evaluate the precision, bias and limits of detection of PIXE as a semi-quantitative method for this application.

Costa et al. [173] report the use of total reflection X-ray fluorescence (TXRF) for the analysis of Na, Mg, Al, K, Ca, Ti, V, Cr, Mn, Ni, Cu, Zn, Rb, Sr, Ba and Pb concentrations in glass samples. The authors report that the limit of detection (LOD) and limit of quantification (LOQ) were "adequate" for determination of trace elements in glass. The authors also evaluated the accuracy and precision of the determination by analysis of

a standard reference materials of glass (NIST 612). The authors report that, for the majority of the elements, good agreement was achieved between the certified value and the value obtained in the NIST 612. The relative standard deviation (RSD%) was achieved between 3.6 and 10.3%. The authors also report no significant differences observed between the proposed method compared to ICP-MS analyses. The TXRF method was applied to the analysis of 31 glass samples and with aid of an exploratory principal component analysis (PCA) resulting in "a perfect discrimination" of the glass from smartphones was obtained. In addition, the authors report that soda-lime glass "could be reasonably distinguished" from smartphone screens.

Sharma et al. [174] report on the use Particle Induced Gamma-ray Emission (PIGE) and Instrumental Neutron Activation Analysis (INAA) for the characterization of windshield glass samples derived from six different vehicle manufactures. PIGE was used to measure the concentrations of the four major elements (Si, Na, Mg and Al) and a total of nineteen (19) elements including sixteen (16) trace elements were analyzed using INAA in a research reactor. The authors used statistical tools such as K-mean, Cluster Analysis and Principal Component Analysis (PCA) for grouping studies. The authors report that the PCA results confirmed that windshield glasses from six manufactures clearly associated to the six different groups.

Almirall et al. [175] reported on the elemental concentration values for seventeen (17) major and trace elements typically present in soda-lime glass manufactured using the "float " process and used in the quantitative analysis and forensic comparison of glass samples using laser ablation (LA) micro sampling coupled to inductively coupled plasma mass spectrometry (ICP-MS). This is the first reporting of the chemical characterization of a new set of float glass standards intended for use as matrix-matched calibration standards in the forensic analysis and comparison of glass by LA-ICP-MS using a standard test method (ASTM E2927-16e1). Three different compositions were manufactured at low, medium, and high concentrations of 32 elements by Corning. This work describes an international collaboration among seven (7) laboratories to evaluate the homogeneity of the three new glass materials and reports the consensus concentrations values of 17 elements at three concentration levels. LA-ICP-MS analysis was reported by eight (8) laboratories and one laboratory reported micro-X-ray Fluorescence Spectrometry data for the same glass standards (CFGS1, CFGS2 and CFGS3). The analytical results reflected <3% relative standard deviation (RSD) within each lab and <5% RSDs among all labs participating in the study for the concentration ranges using sampling spots between 50 μm and 100 μm in diameter. These results suggest that the new calibration standards are homogeneous for most elements at the small sampling volumes (~90 μm deep by ~80 μm in diameter) reported and show excellent agreement among the different participating labs. Consensus concentration values were determined using a previously reported calibration standard (FGS 2) and checked with a NIST 1831 standard reference material.

Becker et al. [176] reported on the use of a single-pulse laser ablation sampling coupled to an inductively coupled plasma time of flight mass spectrometry (Single-Pulse LA-ICP-TOFMS) method in an effort to be able to analyze very small glass samples. The authors compared the results of the single-pulse LA-ICP-TOFMS and report good performance in associating glass fragments from the same source. The authors were able to reduce the necessary sample volume from the typical 400 μm × 200 μm x 100 μm normally used for LA-ICP-MS to 100 μm × 100 μm x 33 μm which corresponds to a reduction in sample mass from ~20 μg to ~0.8 μg. This development allows for the measurement of smaller fragments than previously possible.

Von Wuthenau et al. [177] reported on the use of LA-ICP-MS to analyze glass from perfume bottles to detect counterfeit perfume by comparing authentic perfume glass bottles to the counterfeit glass bottles, without having to open the bottles of perfume. Perfume glass bottles manufactured in different production facilities in Germany, India, Peru and Poland were used for the study. A total of 63 elements could be measured but only 15 elements (Li, Na, Al, Ti, V, Co, Rb, Sr, Mo, Ba, La, Ce, Pr, Er and Pb) were used to associate glass to sources using statistical evaluation of the data (*t*-test, ANOVA, principal component analysis (PCA)). The use of LDA permitted the differentiation of six different production sites from four different countries with a prediction accuracy of 100%.

Martinez-Lopez et al. [178] reported on the use of μ-XRF and LIBS analyses to characterize the homogeneity (elemental variation) of glass compared to the more established method for quantitative analysis using LA-ICP-MS. The aim of the study was to support that the μ-XRF and LIBS methods would produce sufficiently sampling precision (in comparison to LA-ICP-MS) to enable microsampling using μ-XRF and LIBS. The authors report that the variability of the elemental composition within 100 fragments from two different panes of the same windshield was found to be less than 10% RSD for both μ-XRF and LIBS and less than 5% RSD for LA-ICP-MS. Comparison methods simulating casework situations in which one questioned fragment is compared to more than one known fragment resulted in better performance as the number of fragments of the known sample increased (to up to 4 fragments, 12–20 measurements). Error rates below 3% were obtained for μ-XRF and LIBS when selecting the appropriate number of fragments, measurements, and comparison criterion.

1.4.4. Data analysis and interpretation

de Zwart and van Der Weerd [179] reported on the use of filtered contents of a database such that only items that are considered relevant to the population are selected for the background database in the analysis. Six different scenarios related to fibers, textiles, and glass evidence are described along with the hypotheses and relevant populations that may be evaluated by an expert. The focus of the study is to filter items to develop a more relevant population and provide an overview of the selected items and feedback to the examiner.

Rodrigues and Bruni [180] used previously published Energy Dispersive X-ray Fluorescence (EDXRF) data from 28 windshield glass samples from 26 different vehicle models to differentiate between the internal and external panes of the windshield. The oxides of Na, Ca, Mg, Mn, Al, Si, K, Ti and Fe were previously measured by other researchers for both the inner and outer panes of the windshield (for a total of 56 analyses). The authors used unsupervised Principal Component Analysis (PCA) and supervised Soft Interclass Modeling Classification Analogy (SIMCA) methods in the analysis together with Receiver Operating Characteristics (ROC) curves to evaluate the results. The authors report that PCA indicated the presence of two groups of glasses in three main components with the distances and interclass residues in SIMCA showing no outliers. The ROC analysis indicated a sensitivity of 0.793, a specificity of 0.815, and an efficiency of 0.804 for predictions. The authors concluded that this approach was successful in discriminating between the inner and outer panes of the windshields.

Fortunato and Montanari [181] used previously published refractive index and eight metal oxide composition data generated from SEM-EDS analysis of glass fragments to propose the use of a transvariation-based one-class classifier as a measure of typicality in a "one-class" classifier system. The aim of the transvariation-based one-class classifier was to identify the best boundary around the target class, i.e. to recognize as many target objects as possible while rejecting all those deviating from this class.

A presentation by Corzo [182] reported on the use of micro-X-ray Fluorescence Spectrometry (μXRF) analysis of glass samples to develop a database of μXRF data for glass fragments to improve evidence interpretation. The author argues that the development of such a background database can then be used to calculate coincidental match probabilities and likelihood ratios to then assign a significance to the glass evidence.

Malmborg and Nordgaard [183] used the open-source software (SaiLR) to calculate likelihood ratios (LR) from probability distributions of reference data based on SEM-EDS measurements of metal oxides in glass fragments. The authors report that the best performance of the

model was achieved by focusing on the oxides of calcium, magnesium, and silicon. The authors also report that although performance improved with normalization of data, the difference was small. Limits of LR output were set to $1/512 \leq LR \leq 158$ using the empirical lower and upper boundaries (ELUB) LR method. The authors report that the limited range was primarily a consequence of notable within-source variation, but it could also be due to the low discrimination power of the SEM-EDS method to discriminate between glass sources. The authors acknowledge that previous reports using LA-ICP-MS data outperform the reported results. The output from the LR calculation within SaiLR is based on a two-level multivariate kernel density (MVK) model and provides good discrimination between the same and different source comparisons but it does not include a calibration step. The MVK model without calibration has been previously shown to be very sensitive to the dimensionality of the data. The MVK model within SaiLR may be suitable for very low dimension problems (~2–3 variables) but reducing the available number of variables also reduces the discrimination power.

Lucy, Martyna and Curran [184] published an R package, also based on SEM-EDS data, to facilitate the calculation of a multivariate Likelihood Ratio for glass data. This package also uses the MVK model followed by ECE calibration as reported by others.

Park et al. [185] reported a "data in brief" note on the development of a glass "database" constructed of 48 panes of glass produced on consecutive days within a manufacturer and representative glass samples from a second manufacturer. The authors used LA-ICP-MS data from 18 elements using the ASTM E2927 method of analysis. The authors make the raw data available to researchers, but the "database" is not representative of the population of glass as may be needed to calculate significance from coincidental match probabilities and likelihood ratio calculations.

Wen ate al [186] report an alternative continuous Bayesian approach, the Dirichlet Process Mixture Model (DPMM), to model the relevant rarity of glass based on the refractive index (RI) measurements. A DPMM was developed based on a finite mixture model with additional prior specification on the mixture proportions. Glass is a common type of physical evidence in forensic science. The authors report that the key advantage of the method is that it allows for a more flexible model of the probability density distribution of refractive index measurements.

Akmeemana, Corzo and Almirall [187] report the use of a new R-based Shiny graphical user interface (GUI) to calculate calibrated likelihood ratios (LRs) using three (3) different background databases of glass composition measured by LA-ICP-MS using the ASTM E2927 method. The authors also report the development of a new vehicle survey glass database generated at Florida International University (FIU) generated from LA-ICP-MS analysis, a database comprised of a combination of casework and survey samples collected from solution-digestion ICP-MS analysis from the Federal Bureau of Investigation (FBI) Laboratory, and a previously reported casework sample database collected from LA-ICP-MS analysis at the Bundeskriminalamt (BKA) Laboratory. The LRs are calculated using a previously reported two-level multivariate kernel (MVK) model and calibrated using a previously described Pool Adjacent Violators (PAV) algorithm. The log LR (LLR) were calculated and compared to the match criterion recommended in the ASTM E2927-16e1 method, using these three background databases using a typical glass evidence case scenario. This paper also reports how the LLR values increase as the size of the background database increases, as expected.

Almirall and Akmeemana [188] have made available the Shiny Glass application freely through the FIU library for researchers and practitioners to use. The FIU vehicle glass database comprised of more than 330 different vehicle glass samples of known origin and generated using the ASTM E2927 LA-ICP-MS standard method has also been made freely available for download in an effort to encourage future researchers to use LA-ICP-MS data instead of the less discriminating SEM-EDS data commonly used. This R shiny application can be used to calculate the likelihood ratios using a multivariate kernel density (MVK) model. This app was developed to easily access the R code written previously by members of Prof. Almirall's research group at Florida International University. In this procedure, MVK-calculated source likelihood ratios are calibrated using a pool adjacent violators (PAV) algorithm.

Gupta et al. [189] reported on the use of a novel dimensionality reduction method to calculate likelihood ratios (LRs) from multivariate elemental concentrations of glass using LA-ICP-MS data. The LRs were calculated using principal component analysis (PCA) and post hoc calibration steps resulting in very low (<1%) false inclusions when comparing glass samples known to originate from different sources and very low (<1%) false exclusions when comparing glass samples known to originate from the same source. The LRs calculated using the novel PCA approach are compared with previously reported LRs calculated using a more computationally intensive Multivariate Kernel (MVK) model followed by a calibration step using a Pool Adjacent Violators (PAV) algorithm. In both cases, the calibrated LRs limited the magnitude of the misleading evidence, providing only weak to moderate support for the incorrect hypotheses. Most of the different pairs that were found to be falsely included were explained by chemical relatedness (same manufacturer of the glass sources in very close time interval between manufacture). The authors state that the computation of LRs using dimensionality reduction of elemental concentrations using PCA may transfer to other multivariate data-generating evidence types.

When considering only subsets of glass fragments recovered from garments and considering the presence of background glass on garments Vergeer et al. [190] propose to incorporate modelling the probability of an allocation of background fragments into groups given a total number of background fragments by a two-parameter Chinese restaurant process (CRP) for the glass evidence. The proposed solution consists of relaxing the assumption of conditional independence of group sizes of background fragments. Under the assumption of random sampling of fragments to be measured from recovered fragments in the laboratory, parameter values for the Chinese restaurant process may be estimated from a relatively small dataset of glass in other relevant cases. The authors use a dataset of glass fragments collected from upper garments in casework and show model fit to provide a calculation of an LR at activity level accompanied with a parameter sensitivity analysis for reasonable ranges of the CRP parameter values.

Ramos et al. [191] propose models that compare favorably to previously proposed feature-based LR models, by improving the calibration of the computed LRs based on quantitative elemental analysis using LA-ICP-MS and the ASTM E2927 method. The authors assume that the within-source variability is heavy-tailed to incorporate uncertainty when the available data is scarce as it typically happens in forensic glass comparisons. The authors also address the complexity of the between-source variability by the use of probabilistic machine learning algorithms such as a variational autoencoder and a warped Gaussian mixture. The authors report improved overall performance of the likelihood ratios generated by the new model over previously reported approaches and credit the improvement to "a dramatic improvement in the calibration despite some loss in discriminating power".

Corzo et al. [192] report on the results from an interlaboratory study involving seventeen (17) laboratories that participated in three interlaboratory exercises to assess the performance of refractive index, micro X-ray Fluorescence Spectroscopy (micro-XRF), and Laser Induced Breakdown Spectroscopy (LIBS) data for the forensic comparison of glass samples. Glass fragments from automotive windshields were distributed to the participating labs as blind samples and participants were asked to compare the glass samples and report their findings as they would in casework. For samples that originated from the same source, the overall correct association rate was greater than 92% for each of the three techniques (refractive index, micro-XRF, and LIBS). For samples that originated from different vehicles, an overall correct exclusion rate of 82%, 96%, and 87% was observed for refractive index, micro-XRF, and LIBS, respectively. Wide variations in the reported conclusions existed between different laboratories, demonstrating a

need for the standardization of the reporting language used by practitioners. Moreover, few labs used a verbal scale and/or a database to provide a weight to the evidence.

Lambert et al. [193] reported the results of a different interlaboratory study involving ten (10) different laboratories using laser ablation inductively coupled plasma mass spectrometry (LA-ICP-MS) and the standard test method (ASTM E2927-16e1) for the analysis and comparison of glass evidence. The primary aims of the interlaboratory study were to evaluate the performance of the new CFGS2 calibration standard for the quantitative analysis of simulated casework samples, evaluate the comparison criterion as recommended by the ASTM E2927 method and the incorporation of a likelihood ratio (LR) calculation as a more quantitative determination of the strength of evidence. Each laboratory calculated a LR to report the significance of glass source comparisons for a set of glass samples of known origin. Two different types of background databases were used for the calculation of the LR to evaluate the effect of the size and composition of the databases on the calculation of the LR. As expected, glass that originated from the same windowpane was found to be indistinguishable using the ASTM E2927 match criteria and resulted in a high LR value (strong support for an association) and glass that originated from different vehicles are distinguished (strong support for an exclusion). Glass samples that originated from different vehicles but that were the same make, model and year (or comparisons between the inner and outer pane of the same windshield) were chemically similar and reflected a low LR. Good agreement among the laboratories was reported with <5% relative standard deviations (RSDs) among participants.

Akmeemana et al. [194] report on the utility of likelihood ratio (LR) calculations using novel datasets of glass samples of known manufacturing history. The LRs calculated from comparing elemental analysis of glass using ASTM E2927 LA-ICP-MS data for glass manufactured at three different plants over relatively short periods (over 2–6 weeks) range from very low values (LR 10^{-3}) when the glass are manufactured at different plants or manufactured weeks-months apart in the same plant to very high values (LR 10^{3}) when the glass samples are manufactured on the same day. Although the glass samples being compared may not originate from the same broken window source, they do exhibit chemical similarity within these lower and upper bounds and the LRs presented closely correlate chemical relatedness to manufacturing history, specifically the time interval between production.

Acknowledgements

The contribution of Jeff Teitelbaum, Global Forensic and Justice Center at Florida International University is gratefully acknowledged for conducting the initial literature search for articles related to paint, tape, and glass evidence examinations.

References

[1] V.J. Desiderio, C.E. Taylor, N.N. Daéid, in: Handbook of Trace Evidence Analysis, first ed., John Wiley & Sons Ltd, 2021 (Chapter 1): Trace Evidence Recognition, Collection, and Preservation, Schwartz T.R., Rothenberg D.S., Clark B.L. (Chapter 2): Polarized Light Microscopy for the Trace Evidence Examiner, Bowen, A.M. (Chapter 3), Paints and Polymers, Weimer R.B., Wright, D.M., Hodgins, T. (Chapter 6): Interpretation of Glass Evidence, Curran J.M., Hicks T., Trejos, T. (Chapter 7): Interpreting Trace Evidence, Buzzini, P., Curran J.M. Wiley.
[2] R. Dietrich, Paint Analysis: the Handbook for Study and Practice, European Coatings Library, 2021. Vincentz, 2nd ed., Hanover, Germany.
[3] J. Akkerman, T. Biemas, C. Coten, R. Hager, I. Hueben, C. Hoverlmann, J. Krakehl, M. Leute, D. Metach, J. Seewald, A. Thomas, D. Warnon, Resins for Water-Borne Coatings, European Coatings Library, 2021. Vincentz, 1st ed., Hanover, Germany.
[4] J.A. Siegel, K. Mirakovits, Forensic Science: the Basics, 3rd Edition. Chapter 21 Fibers, Paints, and Other Polymers, CRC press, Boca Raton, FL, 2021.
[5] R. Saferstein, T. Roy, Criminalistics: an Introduction to Forensic Science, 13th Edition. Chapter 14. Metals, Paints, and Soil, Pearson, 2021.
[6] K. Sam, T.P. Wampler, Analytical pyrolysis Handbook, in: J.M. Challinor, D. A. DeTata, K.M. Pitts, C. Burnier (Eds.), Chapter 8. Examination of Forensic Evidence, third ed., CRC Press, 2021.
[7] B.P. Wheeler, Practical forensic microscopy: a laboratory manual, in: Chapter 14. Paint Examinations, second ed., John Wiley & Sons Ltd, 2021.
[8] J. Singh, N.R. Sharma, Crime scene management withing forensic science, in: S. Choudhary, A. Ramesh (Eds.), Chapter 5 Paint, Soil, and Glass Evidence: a Silent Witness, Springer, Singapore, 2021.
[9] E.M. Suzuki, Infrared spectroscopy in the forensic sciences A comprehensive discussion, in: Forensic Science Handbook, CRC Press, 2020, pp. 301–423.
[10] D.M. Wright, D.P. Kirby, J.I. Thornton, Forensic paint examination, in: Forensic Science Handbook, CRC Press, 2020, pp. 81–150.
[11] T. Trejos, S. Koch, A. Mehltretter, Scientific foundations and current state of trace evidence—a review, Forensic Chemistry 18 (2020), 100223.
[12] B. Lavine, J. Almirall, C. Muehlethaler, C. Neumann, J. Workman Jr., Criteria for comparing infrared spectra–A review of the forensic and analytical chemistry literature, Forensic Chemistry 18 (2020), 100224.
[13] J.M. Duarte, N.G.S. Sales, M.H. Sousa, C. Bridge, M. Maric, J. de Andrade Gomes, Automotive paint analysis: how far has science advanced in the last ten years? TrAC, Trends Anal. Chem. 132 (2020), 116061.
[14] G. Kaur, Forensic implications of paint, it's use & detection, Int. Med. Leg. Rep. 3 (2) (2020) 34–39.
[15] M.J. Bailey, M. de Puit, F.S. Romolo, Surface analysis techniques in forensic science: successes, challenges, and opportunities for operational deployment, Annu. Rev. Anal. Chem. 15 (2022) 1.1–1.24.
[16] ASTM International, ASTM E2808-21a Standard Guide for Microspectrophotometry in Forensic Paint Analysis, 2021 (West Conshohocken, PA).
[17] ASTM International, ASTM E1610-18 Standard Guide for Forensic Paint Analysis and Comparison, 2018 (West Conshohocken, PA).
[18] ASTM International, ASTM E2937-18 Standard Guide for Using Infrared Spectroscopy in Forensic Paint Examinations, 2018 (West Conshohocken, PA).
[19] ASTM International, ASTM E3234-20 Standard Practice for Forensic Paint Analysis Training Program, 2020 (West Conshohocken, PA).
[20] ASTM International, ASTM E3296-22 Standard Guide for Using Pyrolysis Gas Chromatography and Pyrolysis Gas Chromatography-Mass Spectrometry in Forensic Polymer Examinations, 2022 (West Conshohocken, PA).
[21] ASTM International, ASTM D5380-21 Standard Test Method for Identification of Crystalline Pigments and Extenders in Paint by X-Ray Diffraction Analysis, 2021 (West Conshohocken, PA).
[22] ASTM International, ASTM E3296-22 Standard Guide for Using Pyrolysis Gas Chromatography and Pyrolysis Gas Chromatography-Mass Spectrometry in Forensic Polymer Examinations, 2022 (West Conshohocken, PA).
[23] ASTM International, ASTM E3260-21 Standard Guide for Forensic Examination and Comparison of Pressure Sensitive Tapes, 2021 (West Conshohocken, PA).
[24] ASTM International, ASTM E3233-20 Standard Practice for Forensic Tape Analysis Training Program, 2020 (West Conshohocken, PA).
[25] ASTM International, ASTM E1967-19 Standard Test Method for the Automated Determination of Refractive Index of Glass Samples Using the Oil Immersion Method and a Phase Contrast Microscope, 2019 (West Conshohocken, PA).
[26] ASTM International, ASTM E2330-19 Standard Test Method for Determination of Concentrations of Elements in Glass Samples Using Inductively Coupled Plasma Mass Spectrometry (ICP-MS) for Forensic Comparisons, 2019 (PA).
[27] EPG-BPM-001, Best Practice Manual for the Forensic Examination of Paint, 2022.
[28] EPG Guideline-001, Guideline for the Initial Inspection Search and Recovery of Forensic Paint Samples, 2022.
[29] EPG Guideline-002, Guideline for the Forensic Examination of Paint by FT Infrared Spectroscopy, 2022.
[30] EPG Guideline-003, Guideline for the Forensic Examination of Paint by Raman Spectroscopy, 2022.
[31] EPG Guideline-004, Guideline for the Forensic Examination of Paint by SEM-EDS, 2022.
[32] EPG Guideline-005, Guideline for the Forensic Examination of Paint by Pyrolysis GC-MS, 2022.
[33] F. Kwofie, U.D.N. Perera, M.D. Allen, B.K. Lavine, Application of infrared microscopy and alternating least squares to the forensic analysis of automotive paint chips, J. Chemometr. 35 (1) (2021), e3277.
[34] F. Kwofie, N.U.D. Perera, K.S. Dahal, G.P. Affadu-Danful, K. Nishikida, B. K. Lavine, Transmission infrared microscopy and machine learning applied to the forensic examination of original automotive paint, Appl. Spectrosc. 76 (1) (2022) 118–131.
[35] E.M. Suzuki, Infrared spectra of North American automobile original finishes. X: analysis of perylene pigments—in situ identification of Perylene Red Y (CI Pigment Red 224) and mica based red pearlescent pigments, Forensic Chemistry 25 (2021), 100350.
[36] E.M. Suzuki, Infrared spectra of North American automobile original finishes. XI: in situ identification of perylene pigments—analysis of Perylene Maroon (CI Pigment Red 179) and alumina-based red pearlescent pigments, Forensic Chemistry 25 (2021), 100351.
[37] E.M. Suzuki, Infrared spectra of North American automobile original finishes. XII: analysis of perylene pigments—in situ identification of Perylene Bordeaux (CI Pigment Violet 29), Forensic Chemistry 27 (2022), 100391.
[38] E.M. Suzuki, Infrared spectra of North American automobile original finishes. XIII: analysis of perylene pigments—in situ identification of Perylene Red (CI Pigment Red 178), Forensic Chemistry 29 (2022), 100420.

[39] W.Y. Soong, K.Y. Goh, H. Xie, T.B. Lim, Assessing the automotive paint evidence in Singapore via population and discrimination studies, Forensic Chemistry 21 (2020), 100289.
[40] S. Sharma, R. Chophi, C. Kaur, R. Singh, Chemometric analysis on ATR-FT-IR spectra of spray paint samples for forensic purposes, J. Forensic Sci. 66 (6) (2021), 21902200.
[41] X. He, J. Wang, C. Gao, Y. Liu, Z. Li, N. Li, J. Xia, Differentiation of white architectural paints by microscopic laser Raman spectroscopy and chemometrics, Spectrochim. Acta Mol. Biomol. Spectrosc. 248 (2021), 119284.
[42] J.M. Duarte, N.G.S. Sales, J.W.B. Braga, C. Bridge, M. Maric, M.H. Sousa, J. de Andrade Gomes, Discrimination of white automotive paint samples using ATR-FTIR and PLSDA for forensic purposes, Talanta 240 (2022), 123154.
[43] P. Verma, N. Kaur, P. Soni, Forensic evaluation and comparison of Indian automobile paint chips using FTIR, Mater. Today Proc. 33 (2020) 1727–1732.
[44] N. Kaur, K.S. Abi, P. Verma, M. Mahajan, An elemental analysis of Indian automotive paint using SEM-EDS, Mater. Today Proc. 48 (2022) 1748–1753.
[45] R.Z.R. Sabaradin, R. Osman, Evaluation of evidence value of car primer using pyrolysis-gas chromatography-mass spectrometry (Py-GC-MS) and chemometrics, Sci. Lett. 15 (1) (2021) 43–57.
[46] J. Zięba-Palus, Examination of the variation of chemical composition and structure of paint within a car body by FT-IR and Raman spectroscopies, J. Mol. Struct. 1219 (2020), 128558.
[47] S. Coelho, M.C. de Almeida, C. Família, Vehicle identification from automotive paints transferred in road accidents, Ann. Med. 53 (sup1) (2021) S82–S83.
[48] X. He, J. Wang, B. Zhao, Y. Mu, Y. Liu, W. Hou, T. Ma, Nondestructive discrimination of ship deck paint using attenuated total reflection–Fourier transform infrared (ATR-FTIR) spectroscopy with chemometric analysis, Anal. Lett. 53 (17) (2020) 2761–2774.
[49] C. Wei, J. Wang, A rapid and nondestructive approach for forensic identification of car bumper splinters using attenuated total reflectance Fourier transform infrared spectroscopy and chemometrics, J. Forensic Sci. 66 (2) (2021) 583–593.
[50] W. Qiu, W. Li, Non-destructive characterization and discrimination of vehicle bumpers fragments in forensic science using molecular spectral fusion analysis and chemometrics, Microchem. J. 167 (2021), 106299.
[51] E. Sisco, T.P. Forbes, Forensic applications of DART-MS: a review of recent literature, Forensic Chemistry 22 (2021), 100294.
[52] S. Gupta, N. Samal, Application of direct analysis in real-time mass spectrometry (DART-MS) in forensic science: a comprehensive review, Egypt. J. Food Sci. 12 (1) (2022) 1–25.
[53] N.P. Alderman, M. Courville, R. Tokarczyk, Determination of certain VOCs in paints and architectural coatings by dynamic headspace gas chromatography-mass spectrometry, Anal. Methods 13 (35) (2021) 3894–3899.
[54] M. Tiessen, N.L. Stock, T. Stotesbury, Untargeted SPME–GC–MS characterization of VOCs released from spray paint, J. Chromatogr. Sci. 59 (2) (2021) 103–111.
[55] D.M. Wright, Conducting and reporting paint data Query (PDQ) searches, J. Am. Soc. Trace Evid. Exam. 11 (1) (2021) 3–22.
[56] J.R. Klaasse, L.C. Alewijnse, J. van Der Weerd, TraceBase; A database structure for forensic trace analysis, Sci. Justice 61 (4) (2021) 410–418.
[57] M. Falardeau, C. Muehlethaler, Distribution of aerosol paint droplets in open-and closed-space environments: towards activity level evaluation, Forensic Sci. Int. 306 (2020), 110065.
[58] H. Letendre, K. Séguin, A. Grenier, V. Mousseau, L. Cadola, F. Crispino, First lessons regarding the data analysis of physicochemical traces at activity level in TTADB, J. Can. Soc. Forensic. Sci. 54 (3) (2021) 139–156.
[59] A. Menżyk, A. Martyna, G. Zadora, Evidential value of polymeric materials—chemometric tactics for spectral data compression combined with likelihood ratio approach, Analyst 14220 (2017) 3867–3888.
[60] J. Jordan, R. Helander, P. Laaksonen, Colour stability of wood coatings pigmented with natural indigo from Isatis tinctoria after accelerated weathering, Color. Technol. 138 (2) (2022) 210–218.
[61] P. Sanmartín, J.S. Pozo-Antonio, Weathering of graffiti spray paint on building stones exposed to different types of UV radiation, Construct. Build. Mater. 236 (2020), 117736.
[62] H. Lee, D. Lee, J.M. Seo, Analysis of paint traces to determine the ship responsible for a collision, Sci. Rep. 11 (1) (2021) 1–11.
[63] M.V. de Oliveira Andrade, Forensic analysis of artworks more than a (complex) analytical issue, Braz. J. Anal. Chem. 9 (34) (2022) 10–12.
[64] S. Sirro, K. Ershova, V. Kochemirovsky, J. Fiks, P. Kondrakhina, S. Ermakov, S. Kochemirovskaia, Recognition of fake paintings of the 20th-century Russian avant-garde using the physicochemical analysis of zinc white, Forensic Chemistry 26 (2021), 100367.
[65] R. Chophi, S. Sharma, R. Singh, Discrimination of vermilion (sindoor) using attenuated total reflectance fourier transform infrared spectroscopy in combination with PCA and PCA LDA, J. Forensic Sci. 66 (2) (2021) 594–607.
[66] P. Giménez, A. Linares, C. Sessa, H. Bagán, J.F. García, Capability of Far-Infrared for the selective identification of red and black pigments in paint layers, Spectrochim. Acta Mol. Biomol. Spectrosc. 266 (2022), 120411.
[67] E. Platania, N.L. Streeton, A. Lluveras-Tenorio, A. Vila, D. Buti, F. Caruso, E. Uggerud, Identification of green pigments and binders in late medieval painted wings from Norwegian churches, Microchem. J. 156 (2020), 104811.
[68] C. Rigon, F.C. Izzo, M.L.V.D.Á. Pascual, P. Campíns-Falcó, H. Van Keulen, New results in ancient Maya rituals researches: the study of human painted bones fragments from Calakmul archaeological site (Mexico), J. Archaeol. Sci.: Report 32 (2020), 102418.
[69] J. Walker, R. Hodgkins, B. Berrie, On the surface: reflectance FTIR spectroscopy in cultural heritage research, Microsc. Microanal. 27 (S1) (2021) 2800–2804.
[70] N. Macro, M. Ioele, B. Cattaneo, G. De Cesare, F. Di Lorenzo, M. Storari, M. Lazzari, Detection of bronze paint degradation products in a contemporary artwork by combined non-invasive and micro-destructive approach, Microchem. J. 159 (2020), 105482.
[71] G. Germinario, F. Talarico, M. Torre, Microanalyses and spectroscopic techniques for the identification of pigments and pictorial materials in monet's pink water lilies painting, Microsc. Microanal. 28 (1) (2022) 27–41.
[72] B. Borg, M. Dunn, A.S. Ang, C. Villis, Canvas painting analysis using spectroscopic analysis and microcharacterisation techniques, Sensors 22 (4) (2022) 1442.
[73] S.E. Jorge-Villar, H.G. Edwards, Green and blue pigments in Roman wall paintings: a challenge for Raman spectroscopy, J. Raman Spectrosc. 52 (12) (2021) 2190–2203.
[74] P. Betts, N. Barbi, G. Gates, E. Uffelman, H. Jones, G. Kemeny, Hyperspectral and multispectral reflectance imaging of paintings, Microsc. Microanal. 27 (S1) (2021) 3008–3010.
[75] K. Laclavetine, D. Giovannacci, M. Radepont, A. Michelin, A. Tournié, O. Belhadj, W. Nowik, Macro X-ray fluorescence scanning, multi-and hyperspectral imaging study of multiple layers of paintings on paneled vault in the church of Le Quillio (France), X Ray Spectrom. 50 (4) (2021) 358–374.
[76] J. Brocchieri, L. de Viguerie, C. Sabbarese, M. Boyer, Combination of noninvasive imaging techniques to characterize pigments in Buddhist thangka paintings, X Ray Spectrom. 50 (4) (2021) 320–331.
[77] E. Pouyet, N. Barbi, H. Chopp, O. Healy, A. Katsaggelos, S. Moak, M. Walton, Development of a highly mobile and versatile large MA-XRF scanner for in situ analyses of paintedwork of arts, X Ray Spectrom. 50 (4) (2021) 263–271.
[78] M. Alfeld, MA-XRF for historical paintings: state of the art and perspective, Microsc. Microanal. 26 (S2) (2020) 72–75.
[79] J. Huntley, L.A. Wallis, B. Stephenson, A. Davis, A multi-technique approach to contextualizing painted rock art in the Central Pilbara of Western Australia: integrating in-field and laboratory methods, Quat. Int. 572 (2021) 52–73.
[80] J. La Nasa, P. Carnazza, S. Francone, M.P. Colombini, F. Modugno, Is this tar? Analytical pyrolysis to study the chemical composition of Alberto Burri's paint materials, J. Anal. Appl. Pyrol. 163 (2022), 105483.
[81] J. La Nasa, C. Blaensdorf, E. Dolcher, S. Del Seppia, A. Micheluz, F. Modugno, I. Bonaduce, Historical aircraft paints: analytical pyrolysis for the identification of paint binders used on two Messerschmitt Bf 109 planes, J. Anal. Appl. Pyrol. 163 (2022), 105468.
[82] M. Vermeulen, K. Eremin, G. Rayner, K. Smith, T. Cavanaugh, A. McClelland, M. Walton, Micro reflectance imaging spectroscopy for pigment identification in painting cross sections, Microsc. Microanal. 27 (S1) (2021) 2806–2808.
[83] C. Bouvier, S. Van Nuffel, P. Walter, A. Brunelle, Time-of-flight secondary ion mass spectrometry imaging in cultural heritage: a focus on old paintings, J. Mass Spectrom. 57 (1) (2022), e4803.
[84] A. Botteon, C. Colombo, M. Realini, C. Castiglioni, A. Piccirillo, P. Matousek, C. Conti, Non-invasive and in situ investigation of layers sequence in panel paintings by portable micro-spatially offset Raman spectroscopy, J. Raman Spectrosc. 51 (10) (2020) 2016–2021.
[85] M. Rooney, T. Meldrum, Effect of pigment concentration on NMR relaxometry in acrylic paints, Magn. Reson. Chem. 58 (9) (2020) 880–888.
[86] P. Taugeron, S. Bricaud, C. Kehlet, J. Dittmer, Profiles of paint layer samples obtained in the fringe field of a high field magnet by means of very short broadband frequency-modulated pulses, Magn. Reson. Chem. 58 (9) (2020) 870–879.
[87] G. Tutt, S. Hoffmann, Forensics in motion-Historic vehicles, genuine or fake? Forensic Sci. Int.: Synergy 4 (2022), 100218.
[88] J.S. Kiran, S. Prabhu, Robot nano spray painting-A review, in: IOP Conference Series: Materials Science and Engineering vol. 912, IOP Publishing, 2020, 032044, 3.
[89] B. Zhang, J. Wu, L. Wang, Z. Yu, Accurate dynamic modeling and control parameters design of an industrial hybrid spray-painting robot, Robot. Comput. Integrated Manuf. 63 (2020), 101923.
[90] G. Li, Mechanical, corrosion and cavitation erosion properties of LM 9 grade aluminium-multi-walled carbon nanotubes composites, Aust. J. Mech. Eng. 6 (2) (2020) 1–10.
[91] K.V. Chidhambara, B.L. Shankar, Optimization of robotic spray painting process parameters using taguchi method, in: IOP Conference Series: Materials Science and Engineering vol. 310, IOP Publishing, 2018, 012108, 1.
[92] H. Kim, A.L. Yarin, M.W. Lee, Self-healing corrosion protection film for marine environment, Compos. B Eng. 182 (2020), 107598.
[93] L. Thakur, N. Arora, An investigation on the development and wear performance of chromium-MWCNTs transformed HVOF sprayed nano-WC-CoCr coatings, Surf. Coating. Technol. 388 (2020), 125610.
[94] Y. Zhang, X. Li, J. Zhu, S. Wang, B. Wei, Hybrids of CNTs and acrylic emulsion for the consolidation of wall paintings, Prog. Org. Coating 124 (2018) 185–192.
[95] R.V.S.K. Jakkula, P. Sethuramalingam, Analysis of coatings based on carbon-based nanomaterials for paint industries-A review, Aust. J. Mech. Eng. 129 (2021).
[96] K. Behera, F.C. Chiu, Evident improvements in the rigidity, toughness, and electrical conductivity of PVDF/HDPE blend with selectively localized carbon nanotube, Polym. Test. 90 (2020), 106736.
[97] X. Zeng, Y. Shen, Y. Liu, J. Du, L. Chen, W. Zhou, J. Lin, A cross-linked coating decorated mesh prepared by brush-painting method for oil-in-water emulsions separation, Mater. Chem. Phys. 242 (2020), 122541.
[98] W. Bai, Y. Ma, M. Meng, Y. Li, The influence of graphene on the cathodic protection performance of zinc-rich epoxy coatings, Prog. Org. Coating 161 (2021), 106456.

[99] A.K. Hussain, N. Seetharamaiah, M. Pichumani, C.S. Chakra, Research progress in organic zinc-rich primer coatings for cathodic protection of metals–A comprehensive review, Prog. Org. Coating 153 (2021), 106040.
[100] R. Sukanya, T.N. Barwa, Y. Luo, E. Dempsey, C.B. Breslin, Emerging layered materials and their applications in the corrosion protection of metals and alloys, Sustainability 14 (7) (2022) 1–28, 4079.
[101] S. Li, H. Huang, F. Chen, X. He, Y. Ma, L. Zhang, D. Shchukin, Reinforced anticorrosion performance of waterborne epoxy coating with eco-friendly L-cysteine modified Ti3C2Tx MXene nanosheets, Prog. Org. Coating 161 (2021), 106478.
[102] Y. Wang, W. Chang, Z. Wang, J. Ma, X. Yu, Y. Li, L. Zhang, Silanized MXene/carbon nanotube composites as a shielding layer of polyurethane coatings for anticorrosion, ACS Appl. Nano Mater. 5 (1) (2022) 1408–1418.
[103] C. EzeAgu, Ultra-low-temperature cure for MDF applications, Paints & Coatings Magazine 11 (2021 Nov 11) 5. https://www.pcimag.com/articles/109458-ultra-low-temperature-cure-for-mdf-applications.
[104] J.U. Hong, T.H. Lee, D. Oh, H.J. Paik, S.M. Noh, Scratch-healable automotive clearcoats based on disulfide polyacrylate urethane networks, Prog. Org. Coating 161 (2021), 106472.
[105] G. Cui, C. Zhang, A. Wang, X. Zhou, X. Xing, J. Liu, Q. Lu, Research progress on self-healing polymer/graphene anticorrosion coatings, Prog. Org. Coating 155 (2021), 106231.
[106] C. Zotiadis, I. Patrikalos, V. Loukaidou, D.M. Korres, A. Karantonis, S. Vouyiouka, Self-healing coatings based on poly (urea-formaldehyde) microcapsules: in situ polymerization, capsule properties and application, Prog. Org. Coating 161 (2021), 106475.
[107] D. Czachor-Jadacka, B. Pilch-Pitera, Progress in development of UV curable powder coatings, Prog. Org. Coating 158 (2021), 106355.
[108] K. Diamond, Metallic pigments. Coatings World magazine. https://www.coatingsworld.com/issues/2016-06-01/view_features/metallic-pigmen805413/7880, 2022.
[109] K. Pianoforte, The automotive refinish market. Coatings World magazine. https://www.coatingsworld.com/issues/2015-10-01/view_features/the-automotive-refinish-market/7887, 2022.
[110] N. Thejo Kalyani, A. Jain, S.J. Dhoble, Persistent phosphors for luminous paints: a review, Luminescence 37 (4) (2022) 524–542.
[111] N.F.A. Bakar, M.N.M. Sidek, S.M. Suharman, N. Abd Rahman, Characterization and evaluation of dried automotive paint sludge as cement-based composite, Mater. Today Proc. 63 (1) (2022) S301–S305.
[112] J. Gilbert, Recent trends in architectural coatings. Coatings World magazine March 2022. https://www.coatingsworld.com/issues/2016-09-01/view_features/recent-trends-in-architectural-coatings/7877, 2022.
[113] J. Zieba-Palus, The usefulness of infrared spectroscopy in examinations of adhesive tapes for forensic purposes, Forensic Sci. Criminol 2 (2) (2017) 1–9.
[114] A.H. Mehltretter, M.J. Bradley, D.M. Wright, Analysis and discrimination of electrical tapes: Part I. Adhesives, J. Forensic Sci. 56 (1) (2011) 82–94.
[115] A.H. Mehltretter, M.J. Bradley, D.M. Wright, Analysis and discrimination of electrical tapes: part II. Backings, J. Forensic Sci. 56 (6) (2011) 1493–1504.
[116] A.H. Mehltretter, M.J. Bradley, Forensic analysis and discrimination of duct tapes, Journal of the American Society of Trace Evidence Examiners 3 (1) (2012) 2–20.
[117] C. Nimi, R. Chophi, R. Singh, Discrimination of electrical tapes using ATR-FTIR spectroscopy and chemometrics, J. Forensic Sci. 67 (3) (2022) 911–926.
[118] M. Oliva, D. Zhang, P. Prada-Tiedemann, G. Gamez, Laser assisted sampling vs direct desorption flowing atmospheric pressure afterglow mass spectrometry of complex polymer samples: forensic implications for pressure sensitive tape chemical analysis, Talanta 231 (2021), 122333.
[119] D. Zhang, D. Zeldes, G. Gamez, Three-dimensional mass spectral imaging of polymers via laser-assisted micro-pyrolysis program with flowing atmospheric-pressure afterglow ambient mass spectrometry, Anal. Chem. 94 (7) (2022) 3335–3342.
[120] T. Schoenberger, U. Simmross, C. Poppe, Forensic examination of electrical tapes using high resolution magic angle spinning 1H NMR spectroscopy, Anal. Bioanal. Chem. 408 (1) (2016) 123–129.
[121] M. Prusinowski, A. Mehltretter, C. Martinez-Lopez, J. Almirall, T. Trejos, Assessment of the utility of X-ray Fluorescence for the chemical characterization and comparison of black electrical tape backings, Forensic Chemistry 13 (2019), 100146.
[122] E. Brooks, A. Mehltretter, M. Prusinowski, T. Trejos, Optimization and evaluation of spectral comparisons of electrical tape backings by X-ray fluorescence, Forensic Chemistry 21 (2020), 100291.
[123] C. Martinez-Lopez, T. Trejos, A.H. Mehltretter, J.R. Almirall, Elemental analysis and characterization of electrical tape backings by LA-ICP-MS, Forensic Chemistry 4 (2017) 96–107.
[124] C. Martinez-Lopez, M. Sakayanagi, J.R. Almirall, Elemental analysis of packaging tapes by LA-ICP-MS and LIBS, Forensic Chemistry 8 (2018) 40–48.
[125] C. Martinez-Lopez, T. Trejos, S. Coulson, J. Goodpaster, K. Igowsky, F. Kuczelinis, J.R. Almirall, Interlaboratory evaluations of the performance of elemental analytical methods for the forensic analysis and comparisons of electrical tapes, Forensic Chemistry 12 (2019) 66–77.
[126] A. Gupta, C. Martinez-Lopez, J.M. Curran, J.R. Almirall, Multi-element comparisons of tapes evidence using dimensionality reduction for calculating likelihood ratios, Forensic Sci. Int. 301 (2019) 426–434.
[127] F. Kuczelinis, P. Weis, N.H. Bings, Forensic comparison of PVC tape backings using time resolved LA-ICP-MS analysis, Forensic Chemistry 12 (2019) 33–41.
[128] F. Kuczelinis, J.H. Petersen, P. Weis, N.H. Bings, Calibration of LA-ICP-MS via standard addition using dried picoliter droplets, J. Anal. Atomic Spectrom. 35 (9) (2020) 1922–1931.
[129] E. Brooks, M. Prusinowski, S. Gross, T. Trejos, Forensic physical fits in the trace evidence discipline: a review, Forensic Sci. Int. 313 (2020), 110349.
[130] K.R. McCabe, F.A. Tulleners, J.V. Braun, G. Currie, E.N. Gorecho III, A quantitative analysis of torn and cut duct tape physical end matching, J. Forensic Sci. 58 (2013) S34–S42.
[131] M. Prusinowski, E. Brooks, T. Trejos, Development and validation of a systematic approach for the quantitative assessment of the quality of duct tape physical fits, Forensic Sci. Int. 307 (2020), 110103.
[132] C.D. van Dijk, A. van Someren, R. Visser, M. Sjerps, Evidential value of duct tape comparison using loopbreaking patterns, Forensic Sci. Int. 332 (2022), 111178.
[133] R. Wieten, J. De Zoete, B. Blankers, B. Kokshoorn, The interpretation of traces found on adhesive tapes, Law Probab. Risk 14 (4) (2015) 305–322.
[134] J.A. de Koeijer, M.J. Sjerps, P. Vergeer, C.E. Berger, Combining evidence in complex cases-a practical approach to interdisciplinary casework, Sci. Justice 60 (1) (2020) 20–29.
[135] F. Zapata, F.E. Ortega-Ojeda, C. García-Ruiz, Forensic examination of textile fibres using Raman imaging and multivariate analysis, Spectrochim. Acta Mol. Biomol. Spectrosc. 268 (2022), 120695.
[136] S. Chadwick, M. Lo, F. Brack, J. Bunford, S. Hales, C. Roux, Investigation into the effect of fingermark detection chemicals on the analysis and comparison of pressure-sensitive tapes, Forensic Sci. Int. 315 (2020), 110454.
[137] M. Garcia, V. Gokool, Latent print development on the adhesive side of tape, J. Forensic Ident. 70 (1) (2020).
[138] L. Ostojic, C. O'Connor, E. Wurmbach, Micromanipulation of single cells and fingerprints for forensic identification, Forensic Sci. Int.: Genetics 51 (2021), 102430.
[139] T.T. Tan, P.P. Law, S.W. Kwok, W.W. Yeung, W.C. Ho, W.K. Chung, B.C. Au, A novel solvent-based method to separate duct tape from porous surface for fingerprint development, J. Forensic Sci. 65 (1) (2020) 73–83.
[140] C.M. Gwinnett, A.O. Osborne, A.R. Jackson, The application of tape lifting for microplastic pollution monitoring, Environ. Adv. 5 (2021), 100066.
[141] P. Kanokwongnuwut, K.P. Kirkbride, A. Linacre, An assessment of tape-lifts, Forensic Sci. Int.: Genetics 47 (2020), 102292.
[142] N. Dick, The World of glass 2021 annual report. https://www.glassmagazine.com/article/world-glass-2021-report. (Accessed 23 July 2022).
[143] P. Speaker, Project FORESIGHT annual report 2020-2021. https://researchrepository.wvu.edu/faculty_publications/3093/. (Accessed 24 July 2022).
[144] S. Choudhary, A. Ramesh, Paint, soil, and glass evidences: a silent witnesses, in: Crime Scene Management within Forensic Science, Springer, Singapore, 2021, pp. 107–127.
[145] P.D. Tiffany Roy, Matter, light, and glass examination, richard Saferstein, in: Criminalistics an Introduction to Forensic Science, Pearson, 2021.
[146] J.A.S. Mirakovits, Glass and Soil Kathy in *Forensic Science the Basics*, vol. 4, CRC Press, 2022.
[147] J. Curran, T. Hicks, T. Trejos, Interpretation of glass evidence, Handb. Trace. Evid. Anal. (2020) 377–420.
[148] B.P. Wheeler, Experiment 19 glass breakage determinations, in: Practical Forensic Microscopy: A Laboratory Manual, Wiley, 2021.
[149] B.P. Wheeler, Experiment 19A glass examinations, in: Practical Forensic Microscopy: A Laboratory Manual, Wiley, 2021.
[150] Nadarajan, D., Daud, S. M. S. M., & Shariff, N. S. M. Analysis of Glass Fracture Pattern on Soda Lime and Tempered Glass Caused by Shotgun Bullet Impact.
[151] A. Butt, A. Ali, A. Ahmad, M. Shehzad, A. Malik, Forensic investigation of bullet holes for determining distance from glass fracture analysis, Austin J. Forensic Sci. Criminol. 8 (1) (2021) 1085.
[152] M.G. Haag, L.C. Haag, Projectiles and glass, in: Shooting Incident Reconstruction, Academic press, 2020.
[153] J.J. Beach, The Relationship between Impact Energy and Glass Fracture via. 177 Caliber Steel BBs, City University of New York John Jay College of Criminal Justice, 2020.
[154] S. Dondeti, H.V. Tippur, Crack initiation and slow growth in soda-lime glass from a self-healed crack, Theor. Appl. Fract. Mech. 119 (2022), 103341.
[155] B. Jiang, M. Atif, Y. Ding, Y. Guo, Y. Li, An experimental study on the dynamic flexural tensile behavior of glass, Eng. Fract. Mech. 266 (2022), 108417.
[156] B. Grant, G. Sauzier, S.W. Lewis, Discrimination of automotive window tint using ATR-FTIR spectroscopy and chemometrics, Forensic Sci. Int. 313 (2020), 110338.
[157] L. Viviani, M. Di Paola, G. Royer-Carfagni, A fractional viscoelastic model for laminated glass sandwich plates under blast actions, Int. J. Mech. Sci. 222 (2022), 107204.
[158] T. Vörös, K. Takács, A. Szabó, A. Krizsán, Forensic investigation of glass microfragments exposed to heat, Forensic Sci. Int. 334 (2022), 111265.
[159] R. Podor, F. Méar, J. Lautru, S. Schuller, L. Montagne, Glass reactivity at high temperature, Microsc. Microanal. 27 (S2) (2021) 49–50.
[160] C. Nentwig, A. Schutz, S. Steinhoff, J. Adamec, S.N. Kunz, Forensic and biomechanical aspects of used, empty 0.5 l beer glass bottles as a striking weapon against the skull, Rechtsmedizin 31 (6) (2021) 494–500.
[161] G.Z. Thompson, B. Dawood, T. Yu, B.K. Lograsso, J.D. Vanderkolk, R. Maitra, A. F. Bastawros, Fracture Mechanics-Based Quantitative Matching of Forensic Evidence Fragments, 2021 *arXiv preprint arXiv:2106.04809*.
[162] T. Vörös, K. Takács, Refractive index measurement of the smallest bulk and surface glass microfragments in a model case, J. Forensic Sci. 66 (5) (2021) 1948–1955.

[163] T. Vörös, K. Takács, P. Reger, Refractive index variations of glass microfragments by annealing–forensic applications, Epitoanyag-J. Silic. Based. Compos. Mater. 72 (6) (2020).
[164] T. Ernst, K. Gates, C. Gregory, Hamburg, Forensic. Exam. Ceramic Frit. Automot. JASTEE. 10 (1) (2020) 22–44.
[165] S. Cagno, G. Van der Snickt, S. Legrand, J. Caen, M. Patin, W. Meulebroeck, K. Janssens, Comparison of four mobile, non-invasive diagnostic techniques for differentiating glass types in historical leaded windows: MA-XRF, UV–Vis–NIR, Raman spectroscopy and IRT, X Ray Spectrom. 50 (4) (2021) 293–309.
[166] J. Wimpenny, G.R. Eppich, N. Marks, F. Ryerson, K.B. Knight, Characterizing major and trace element compositions in fallout melt glass from a near-surface nuclear test, J. Environ. Radioact. 243 (2022), 106796.
[167] M. Jacquemin, P. Simon, A. Canizares, L. Hennet, C. Bessada, D. Skrelic, E. Burov, High-sensitivity Raman imaging of the surface of casted glass plates, J. Raman Spectrosc. 52 (5) (2021) 1048–1054.
[168] V. Merk, D. Huber, L. Pfeifer, S. Damaske, S. Merk, W. Werncke, M. Schuster, Discrimination of automotive glass by conjoint Raman and laser-induced breakdown spectroscopy and multivariate data analysis, Spectrochim. Acta B Atom Spectrosc. 180 (2021), 106198.
[169] R. Corzo, E. Steel, Improving signal-to-noise ratio for the forensic analysis of glass using micro X-ray fluorescence spectrometry, X Ray Spectrom. 49 (6) (2020) 679–689.
[170] S.K. Samanta, T.N. Nag, V. Sharma, R. Tripathi, R. Acharya, P.K. Pujari, Intercomparison studies of Instrumental Neutron Activation Analysis using singles and gamma–gamma coincidence spectrometry for trace element determination in sodalime glass and sediment matrices and utilization of coincidence method for rapid automobile glass forensics, Nucl. Instrum. Methods Phys. Res. Sect. A Accel. Spectrom. Detect. Assoc. Equip. 1006 (2021), 165429.
[171] O. Kaspi, O. Girshevitz, H. Senderowitz, PIXE based, Machine-Learning (PIXEL) supported workflow for glass fragments classification, Talanta 234 (2021), 122608.
[172] O. Kaspi, O. Israelsohn-Azulay, Y. Zidon, H. Rosengarten, M. Krmpotić, S. Gouasmia, H. Senderowitz, Inter-laboratory workflow for forensic applications: classification of car glass fragments, Forensic Sci. Int. 333 (2022), 111216.
[173] C.L. Costa, C.T. Prais, C.C. Nascentes, A simple method for glass analysis using total reflection X-ray fluorescence spectrometry, Talanta 243 (2022), 123354.
[174] V. Sharma, A. Sarkar, R. Acharya, H.K. Bagla, P.K. Pujari, Utilization of accelerator and reactor based nuclear analytical techniques for chemical characterization of automobile windshield glass samples and potential of statistical analyses using trace elements towards glass forensics, Forensic Sci. Int. 334 (2022), 111262.
[175] J. Almirall, A. Akmeemana, K. Lambert, P. Jiang, E. Bakowska, R. Corzo, P. Zoon, Determination of seventeen major and trace elements in new float glass standards for use in forensic comparisons using laser ablation inductively coupled plasma mass spectrometry, Spectrochim. Acta B Atom Spectrosc. 179 (2021), 106119.
[176] P. Becker, C. Neff, S. Hess, P. Weis, D. Günther, Forensic float glass fragment analysis using single-pulse laser ablation inductively coupled plasma time of flight mass spectrometry, J. Anal. Atomic Spectrom. 35 (10) (2020) 2248–2254.
[177] K. von Wuthenau, T. Segelke, A. Kuschnereit, M. Fischer, Glass authentication: laser ablation-inductively coupled plasma mass spectrometry (LA-ICP-MS) for origin discrimination of glass bottles, Talanta 235 (2021), 122686.
[178] C. Martinez-Lopez, O. Ovide, R. Corzo, Z. Andrews, J.R. Almirall, T. Trejos, Homogeneity assessment of the elemental composition of windshield glass by μ-XRF, LIBS and LA-ICP-MS analysis, Forensic Chemistry 27 (2022), 100384.
[179] D. de Zwart, J. van Der Weerd, Extraction of the relevant population from a forensic database, Sci. Justice 61 (4) (2021) 419–425.
[180] C.H. Rodrigues, A.T. Bruni, Automobilistic glasses as crime scene traces: a multivariate approach, Quím. Nova 44 (2021) 553–560.
[181] F. Fortunato, L. Anderlucci, A. Montanari, One-class classification with application to forensic analysis, J. Roy. Stat. Soc. C 69 (5) (2020) 1227–1249.
[182] R. Corzo, The use of an XRF glass database to assign a significance to forensic evidence, Microsc. Microanal. 27 (S1) (2021) 1290–1291.
[183] J. Malmborg, A. Nordgaard, Validation of a feature-based likelihood ratio method for the SAILR software. Part II: elemental compositional data for comparison of glass samples, Forensic Chemistry 27 (2022), 100385.
[184] D. Lucy, S.A. Martyna, J. Curran, Comparison: multivariate likelihood ratio calculation and evaluation, R package version 1.0-5 (2020). https://CRAN.R-project.org/package=comparison.
[185] S. Park, A. Carriquiry, L.K. Horkley, D.W. Peate, A database of elemental compositions of architectural float glass samples measured by LA-ICP-MS, Data Brief 30 (2020), 105449.
[186] Z. Wen, J.M. Curran, S.A. Harbison, G. Wevers, Bayesian mixture modelling for glass refractive index measurement, Sci. Justice 61 (4) (2021) 345–355.
[187] A. Akmeemana, R. Corzo, J. Almirall, Calculation of likelihood ratios in forensic glass comparisons; introduction to a R code and Shiny app applied to existing background glass elemental databases, Forensic Chemistry 27 (2022), 100390.
[188] J. Almirall, A. Akmeemana, Shiny glass application, FIU Research Data Portal, V1, UNF:6:2XbMxhzvvWpDBHmNtsHcOw== [fileUNF], https://doi.org/10.34703/gzx1-9v95/OB8BS9, 2022.
[189] A. Gupta, R. Corzo, A. Akmeemana, K. Lambert, K. Jimenez, J.M. Curran, J. R. Almirall, Dimensionality reduction of multielement glass evidence to calculate likelihood ratios, J. Chemometr. 35 (1) (2021), e3298.
[190] P. Vergeer, A.J. Leegwater, K. Slooten, Evaluation of glass evidence at activity level: a new distribution for the background population, Forensic Sci. Int. 316 (2020), 110431.
[191] D. Ramos, J. Maroñas, J. Almirall, Improving calibration of forensic glass comparisons by considering uncertainty in feature-based elemental data, Chemometr. Intell. Lab. Syst. 217 (2021), 104399.
[192] R. Corzo, T. Hoffman, T. Ernst, T. Trejos, T. Berman, S. Coulson, J. Almirall, An interlaboratory study evaluating the interpretation of forensic glass evidence using refractive index measurements and elemental composition, Forensic Chemistry 22 (2021), 100307.
[193] K. Lambert, S. Montero, A. Akmeemana, R. Corzo, G. Gordon, E. Haase, J. Almirall, An interlaboratory study to evaluate the forensic analysis and interpretation of glass evidence, Forensic Chemistry 27 (2022), 100378.
[194] A. Akmeemana, P. Weis, R. Corzo, D. Ramos, P. Zoon, T. Trejos, J. Almirall, Interpretation of chemical data from glass analysis for forensic purposes, J. Chemometr. 35 (1) (2021), e3267.